Draft July 27, 2010
Preprint typeset using LaTeX style emulateapj v. 11/10/09

SHORT GAMMA-RAY BURSTS FROM DYNAMICALLY-ASSEMBLED COMPACT BINARIES IN GLOBULAR CLUSTERS: PATHWAYS, RATES, HYDRODYNAMICS AND COSMOLOGICAL SETTING

William H. Lee[1], Enrico Ramirez-Ruiz[2], and Glenn van de Ven[3,4]
[1]Instituto de Astronomía, UNAM, Apdo. Postal 70–264, Cd. Universitaria, México DF 04510; wlee@astroscu.unam.mx
[2]Department of Astronomy and Astrophysics, University of California, Santa Cruz, CA 95064; enrico@ucolick.org
[3]Max Planck Institute for Astronomy, Königstuhl 17, 69117 Heidelberg, Germany; glenn@mpia.de and
[4]Institute for Advanced Study, Einstein Drive, Princeton, NJ 08540, USA; Hubble Fellow

Draft July 27, 2010

ABSTRACT

We present a detailed assessment of the various dynamical pathways leading to the coalescence of compact objects in Globular Clusters (GCs) and Short Gamma-Ray Burst (SGRB) production. We consider primordial binaries, dynamically formed binaries (through tidal two-body and three-body exchange interactions) and direct impacts of compact objects (WD/NS/BH). Here we show that if the primordial binary fraction is small, close encounters dominate the production rate of coalescing compact systems. We find that the two dominant channels are the interaction of field NSs with dynamically formed binaries, and two-body encounters. Under such conditions, we estimate the redshift distribution and host galaxy demographics of SGRB progenitors, and find that GCs can provide a significant contribution to the overall observed rate.

Regarding the newly identified channel of close stellar encounters involving WD/NS/BH, we have carried out precise modeling of the hydrodynamical evolution, giving us a detailed description of the resulting merged system. Our calculations show that there is in principle no problem in accounting for the global energy budget of a typical SGRB. The particulars of each encounter, however, are variable in several aspects, and can lead to interesting diversity. First and most importantly, the characteristics of the encounter are highly dependent on the impact parameter. This is in contrast to the merger scenario, where the masses of the compact objects dictate a typical length and luminosity scale for SGRB activity. Second, the nature of the compact star itself can produce very different outcomes. Finally, the presence of tidal tails in which material will fall back onto the central object at a later time is a robust feature of the present set of calculations. The mass involved in these structures is considerably larger than for binary mergers. It is thus possible to account generically in this scenario for a prompt episode of energy release, as well as for activity many dynamical time scales later.

Subject headings: gamma rays: bursts — stars: neutron — hydrodynamics — accretion disks — gravitational waves — globular clusters

1. INTRODUCTION

Until fairly recently, SGRBs were known predominantly as bursts of γ-rays, and largely devoid of observable traces at lower energies. The launch and successful operation of the *Swift* satellite has now enabled the detection and localization of X-ray afterglows from several events, enabling in turn the study of their properties at optical and radio wavelengths and the identification of the host galaxies at cosmological distances (Berger et al. 2005; Fox et al. 2005; Barthelmy et al. 2005; Hjorth et al. 2005; Gehrels et al. 2005; Bloom et al. 2006; Prochaska et al. 2006). The occurrence of a fraction of events among old stellar populations e.g., of an elliptical galaxy for GRB 050724, rules out a source uniquely associated with recent star formation. In addition, no bright supernova is observed to accompany SGRBs, contrary to what is seen in most nearby long-duration GRBs. It is clear by now that short and long events are not drawn from the same parent stellar population, and that SGRBs are far from standard (Nakar 2007; Gehrels, Ramirez-Ruiz & Fox 2009). This hints at the underlying possibility that the progenitor itself may be quite different from burst to burst, and not entirely restricted to the most widely favoured scenario involving the merger of close binaries (e.g. Paczyński 1986; Eichler 1989) containing neutron stars (NS) and/or black holes (BH).

Since the first evidence from the *Uhuru* and OSO-7 satellites revealed a population of highly luminous low-mass X-ray binaries (LMXBs) in globular clusters (GCs), it has been noted that the formation rate per unit mass of these objects is orders of magnitude higher in GCs than in the Galactic disk (Katz 1975; Clark 1975). This discovery stimulated a flurry of theoretical work into the formation of GCs LMXBs by the processes of two- and three-body encounters(Fabian et al. 1975; Heggie 1975; Hills 1975). These dynamical formation scenarios are a natural explanation for the high occurrence of LMXBs in GCs since the stellar densities, and hence encounter rates, are much higher in the cores of GCs than other regions of the Galaxy (Pooley et al. 2003; Heinke et al. 2006). In such environments, in fact, it is unavoidable that many stars undergo close encounters and even physical collisions, with high probability, within their lifetimes (see e.g., Rosswog et al. 2009; Raskin et al. 2009). It is the interplay between compact stars in such dense environments and their ability to trigger SGRBs that forms the main topic of this paper.

In general, forming a compact binary system requires some mechanism to dispose of enough energy to effec-

tively bind them. Two such processes have been considered for conditions in globular clusters (Hut & Verbunt 1983). The first is the presence of an additional star which can carry away some energy in kinetic form. This has been considered by Grindlay et al. (2006) as a plausible SGRB channel by computing the outcomes of exchange interactions between binaries containing one compact object and a single neutron star in a collapsed GC core. The second is the loss of energy to internal stellar oscillations, excited by the tidal forces of one star on the other.

Here we suggest an alternative and perhaps less restrictive mechanism for SGRB production related to the second mechanism given above, namely, the tidal capture and collision of compact objects in dense stellar environments. In this new scenario, the compact objects are contained within a globular cluster, and interact directly through close encounters rather than being driven together by pure gravitational wave emission in existing close binaries. Event rates for such interactions within galaxies have been found to be much too low to be of interest (Janka & Ruffert 1996) when compared with the GRB event rate, but they may be frequent enough to have an important effect on their production in GCs[1]. In this paper we make a careful assessment of the various dynamical evolutionary pathways involving compact objects in such environments, focusing particularly on the frequency and physical character of the tidal capture of two compact objects that are ultimately capable of leading to a merger and thus powering a gamma-ray burst. We find that they can provide a substantial contribution to the total rate, and compute the evolution of the associated rates with redshift.

Some pressing questions include: When would two passing relativistic stars capture each other in a bound close orbit? When two neutron stars collide, does the rapidly-spinning merged system have too much mass (for most presumed equations of state) to form a single stable object? If so, the expected outcome after a few milliseconds would therefore be a spinning BH, orbited by a torus of neutron-density matter. When a NS collides with a BH, does enough mass remain in the orbiting debris to catalyze the extraction of energy from the hole at a rate adequate to power a short-lived GRB? How do the long tidal tails thrown out through the outer Lagrange point affect the accretion stream around the primary star? Even if the evolution time scale for the bulk of the debris torus were no more than a second, is enough mass and energy still available to power the late time flares? What is the relative frequency and observable signatures of all these collision events and how do they compare to *Swift* observations?

The structure of this paper is as follows: detailed hydrodynamic simulations of encounters of compact objects of various types and with varying impact parameters are presented in Section 2 together with a detailed description of the numerical methods and the initial models; the resulting gravitational wave signals are shown in Section 3; Section 4 offers an estimate of the encounter rate as function of cosmic time, and compares it with the merger rate of compact binaries. We discuss our findings in Section 5, and we summarize and conclude in Section 6.

[1] Hansen & Murali (1998) have proposed collisions of compact objects with main sequence stars as possibly relevant for the production of GRBs in GCs, although it is not clear how the large baryon loading problem could be circumvented in this case

2. DYNAMICS OF TIDAL CAPTURE AND DISRUPTION

2.1. *Numerical implementation*

The hydrodynamical calculations shown subsequently have been performed with the three dimensional Smooth Particle Hydrodynamics (SPH) code previously used to study merging double neutron star and black hole–neutron star binaries (Monaghan 1992; Lee & Kluzniak 1999). The problem does not allow for simplifications due to symmetry and SPH, being a Lagrangian scheme lends itself particularly well to this kind of situation. The tidal tails seen in binary mergers [see e.g. Rasio & Shapiro (1994); Lee (2001); Rosswog et al. (2003)] are a natural outcome in the present scenario as well, and following their formation and evolution is one of the main objectives here, which is not possible with grid–based codes. Self–gravitating spherical stars of a given mass, M, and radius, R, in hydrostatic equilibrium with a polytropic pressure–density relation $P = K\rho^{\Gamma}$, where K and Γ are constants, are constructed with $N \simeq 10^5$ fluid elements (SPH "particles") and used for the dynamical evolution. We have performed test simulations with varying spatial resolution to test for convergence, using from $N \simeq 10^4$ to $N \simeq 2 \times 10^5$ SPH particles. We are here mainly interested in the dynamics of the disruption process for a limited number of dynamical times, and have found that $N \simeq 10^5$ particles are sufficient for this purpose. We thus report all simulations at this initial uniform resolution level. Our calculations are Newtonian, so we cannot model a true black hole. We merely approximate one as a point mass $M_{\rm BH}$, any matter approaching within a Schwarzschild radius $r_{\rm Sch} = 2GM_{\rm BH}/c^2$ being accreted (and its mass added to that of the hole). Clearly this is a problem that ideally should be treated in full General Relativity, but a first understanding can be gained with the use of this approach. We note that previous work on coalescing black hole-neutron star binaries (Lee, Ramirez-Ruiz & Granot 2005; Rosswog 2005) has made use of the pseudo-Newtonian potential of Paczyński & Wiita (1980) for the black hole, which reproduces the existence and position of a last stable orbit for test particles in circular orbits around a Schwarszchild black hole. Doing this thus requires considering fairly small mass ratios, a condition which is not met in the present set of calculations, with the additional complication of highly eccentric orbits for the parabolic encounters of interest. We have hence elected to keep to a purely Newtonian formulation which, albeit simplistic, is quantifiably so.

For neutron stars, most equations of state reveal that the radius varies little over a range of masses. In the case of polytropes, the mass–radius relation is $R \propto M^{(\Gamma-2)/(3\Gamma-4)}$, so if the adiabatic index is $\Gamma = 2$, the radius is only a function of the structure constant K and the central density, $\rho_{\rm c}$. Our standard "neutron star" is thus a spherical, non–spinning polytrope with $\Gamma = 2$, $M_{\rm NS} = 1.4M_{\odot}$ and $R_{\rm NS} = 13.4$ km. In order to investigate the effects of a different compressibility, we have also considered a neutron star with index $\Gamma = 5/3$ of

the same mass and radius for certain orbital parameters, detailed below. We have also considered the case of a low–mass white dwarf ($M_{\rm WD} = 0.5 M_\odot$) interacting with a black hole. In this case it is appropriate to use the equation of state for a cold non–relativistic Fermi gas, $P = K_{\rm n.r.}\rho^{5/3}$, giving a radius $R_{\rm WD} = 1.1 \times 10^4$ km.

Three-dimensional calculations of binary interactions are typically evolved for only a few tens of milliseconds, and during this short time large scale gravitational dynamics determine the final state of the system. Once the initial conditions are set, we use a simple ideal gas equation of state, where the pressure is given by $P = \rho u(\Gamma - 1)$ and u is the specific internal energy, to follow the thermodynamics of the gas, with no heating or cooling mechanisms present. Shocks are allowed to form in the usual numerical way (through an artificial viscosity), and are the only source of local dissipation.

The single additional ingredient that is necessary in terms of global dissipation is the emission of gravitational waves, since it can (and does) affect the orbital evolution. For binary mergers, the point–mass approximation in the weak field limit is often used to compute an effective drag, removing angular momentum and energy from the system. It is switched off once the stars come into contact, or if one of them is tidally disrupted. However, for the present set of calculations on various orbits it is not a good approximation. Rather, we require an expression for the energy loss rate of extended bodies, which can be used for more general trajectories (for example initially parabolic). We thus compute the rate of energy loss as

$$\frac{dE_{\rm GW}}{dt} = \frac{1}{5}\frac{G}{c^5}\left[\frac{d\ddot{I}_{jk}}{dt}\frac{d\ddot{I}_{jk}}{dt}\right], \qquad (1)$$

where I_{jk} is the traceless mass quadrupole moment. The first two time derivatives can be easily calculated without having to perform two numerical time derivatives explicitly with the use of the continuity and Euler equations (Rasio & Shapiro 1992; Lee & Kluzniak 1999). The third derivative requires numerical treatment, and numerical noise in its calculation can be reduced by interpolation over neighboring points in the evolution. We have tested this implementation by computing the evolution of binaries with large separations, where the orbital decay time scale is much longer than the orbital period, and find excellent agreement with the point-mass formula for circular orbits. It is important to consider this more accurate treatment for parabolic encounters, since the energy loss rate at periastron can be substantially larger (by a factor of 2-3, depending on the impact parameter) than that estimated from the expression for point masses in circular orbits, leading to different, and overall, faster encounters. In addition, the effect on the loss rate because of the formation of tidal bulges on the stars is automatically taken into account, since it is the full fluid quadrupole moment that is used in computing the loss rate.

2.2. *Conditions for stellar encounters*

The stellar velocity dispersion in GCs is insignificant when compared to that acquired from the mutual gravitational acceleration of two compact, stellar mass objects as they approach each other. It is thus reasonable to assume at first that encounters will be parabolic, i.e., with vanishing orbital energy, E, at infinity. However the impact parameter, b, may vary, and is related to the total orbital angular momentum, L, in the two–body system.

When the separation between the two masses, a, is large compared to their individual radii, $R_{\rm i}$, we may safely consider that they behave as point particles and compute the orbit accordingly. It is only when these quantities become comparable that finite–size effects need to be considered, and a full hydrodynamic calculation must be performed. It has been shown for the case of compact binary *mergers* that tidal effects can de-stabilize the orbit even in the absence of relativistic considerations at small enough separations (Lai et al. 1993a,b; Rasio & Shapiro 1994). The orbital decay rate thus induced is comparable to that due to gravitational radiation back reaction, and can even dominate the evolution for the last few cycles. The equation of state plays a role in the magnitude and growth of this effect, and for neutron stars it is almost certainly generically important. We have thus elected to study collisions by placing the stars (whether they are black holes, neutron stars or white dwarfs) initially at separations comparable to those used in merger calculations. This choice is always a trade-off, since using a larger separation will always be more accurate, at the cost of added computational effort (during which the components approach each other with little visible evolution). The point worth noting here is that as a result of tidal effects, a bulge will form on each star as they approach, but will slowly fall behind the line joining the centers. At periastron, a significant lag angle may have developed, and this can have an effect on the subsequent evolution of the material, through the action of gravitational torques by the more massive primary on the lighter, bar–like secondary. For the present set of calculations we have chosen to use spherical, non-perturbed stars for initial conditions. A solution in terms of compressible tri–axial ellipsoids is possible for the previous evolution (Lai et al. 1993b), but given our overall simplifications we believe this will not affect our results significantly. At the chosen initial separations, the induced tidal bulges and lag angles are still quite small[2].

A convenient way to parameterize the encounters is by comparing the strength of the tidal field produced by the primary to the self gravity of the secondary, through

$$\eta = \left(\frac{M_2}{M_1}\frac{R_{\rm p}^3}{R_2^3}\right)^{1/2}, \qquad (2)$$

where M_1 and M_2 are the primary and secondary mass, $R_{\rm p}$ is the periastron distance, and R_2 is the radius of the secondary. With this definition, at a fixed mass ratio $q = M_2/M_1 \leq 1$, encounters with $\eta \gg 1$ have large impact parameters, while $\eta \simeq 1$ marks collisions where the secondary is tidally disrupted because the tidal field has become as intense as that holding the star together. An important difference between encounters with components of similar mass and those in which $q \ll 1$, as

[2] A detailed comparison of the differences between the use of spherical stars as opposed to tri–axial ellipsoids was carried out in the case of mergers (Lee 2000, 2001). Overall, results differed by less than $\approx 5\%$ for the equation of state used here with $\Gamma = 2$.

for the disruption of stars by supermassive black holes in AGN (Frank 1978; Lacy et al. 1982; Carter & Luminet 1983; Rees 1988), is that the periastron distance is much smaller in the former, and in fact comparable to the stellar radius. For a given intensity of the encounter, the periastron distance can be written as

$$R_{\rm p} = R_2 \eta^{2/3} q^{-1/3}. \quad (3)$$

Thus for a disruptive encounter with $\eta \simeq 1$, $R_{\rm p} \simeq 200 R_2$ if $q = 10^{-7}$, but $R_{\rm p} \simeq 2R_2$ for $q \simeq 1/3$. In the first case the disruption is a purely gravitational encounter, while in the second it is additionally a direct collision, which may modify the mass ratio substantially *during* the encounter.

The parameter η can also be thought of as the ratio between the dynamical time scale of the star (or its rotational break up period) and the duration of the encounter. Thus for the intrinsic spin of the secondary to be of any relevance, it must be rotating near the Keplerian limit. The most rapidly spinning neutron stars detected in LMXBs in our galaxy (Backer et al. 1982) and in GCs (Hessels et al. 2006) are clearly below this threshold, by a factor 3-5, depending on the assumed equation of state. It is thus reasonable to assume that in most cases the neutron star spin is negligible for the purposes of the encounters considered here, and we do so in what follows.

2.3. *Tidal capture and the formation of close binaries*

When two compact stars pass close to each other so that $\eta \simeq 1$, the tidal perturbations produce accelerations of the stellar material relative to the stellar center. The internal energy gained by the stars is taken from the kinetic energy of their relative motion. While the internal energy $\Delta E_{\rm T}$ gained by each component is a small fraction of the star's internal energy, it can be comparable with the kinetic energy of relative motion of the two bodies at large separation. The two stars will thus become bound if enough energy is absorbed in exciting the oscillations. The resulting elliptical orbit immediatey after capture will have an initial eccentricity only slightly less than unity. However, there will be many successive passages at about the same periastron distance, and these will lead to further energy transfer. Ultimately the orbit should become nearly circular.

The value of $\Delta E_{\rm T}$ and thus the resultant condition for tidal capture may be determined by requiring that the frequency of the perturbation be slightly smaller than the natural frequencies of the perturbed system. The tidal field excites non-radial modes of oscillation in the secondary and, while there are many of these, those most effectively excited have the smallest number of nodes, with an angular frequency $\omega_{\rm osc}$ that is usually some two to three times $\omega_2 = (GM_2/R_2^3)^{1/2}$. Now, the angular frequency of the encounter $\omega_{\rm p}$ is effectively $V_{\rm p}/R_{\rm p}$ and can be written as $\omega_{\rm p} \approx 2\omega_2 (R_2/R_{\rm p})^{3/2}$. Thus for $R_{\rm p}/R_2 = 2$, $\omega_{\rm p}/\omega_{\rm osc} \approx 0.3$ for the lowest modes. However, for $R_{\rm p}/R_2 = 10$, $\omega_{\rm p}/\omega_{\rm osc} \approx 0.03$. For such slow changes, the shape of each star will adjust to the changing form of the equipotential surfaces and the net heating is markedly reduced. The binaries formed by tidal capture are thus generally very hard.

Since the fraction of the initial angular momentum which is transferred to stellar rotation can scarcely exceed a few percent because of the relatively small stellar radius of gyration, one can assume that the orbital angular momentum remains roughly constant. Hence in a circular orbit of radius $R_{\rm c}$ and relative velocity $V_{\rm c}$, $R_{\rm c}V_{\rm c}$ must equal the initial $R_{\rm p}V_{\rm p}$. With $V_{\rm p}$ obtained by the condition that $(1/2)\mu_{\rm r}V_{\rm p}^2 = GM_2^2/R_{\rm p}$, where $\mu_r = M_1M_2/(M_1+M_2)$ and $V_{\rm c}$ computed from force balance in a circular orbit, one finds $R_{\rm c} = 2R_{\rm p}$. To obtain more exact results for the resulting conditions for tidal capture, the excitation of the individual normal modes must be considered, and the heating summed over all modes. Analysis of this effect by Press & Teukolsky (1977) has taken the parabolic motion of the two stars accurately into account, but in the tidal potential only terms varying as $1/r^2$ and $1/r^3$ have been considered, an approximation valid for $R_{\rm p}/R_2 \geq 3$. Detailed calculations were first carried out using linear theory for $\Gamma = 4/3$ (Press & Teukolsky 1977; Lee & Ostriker 1986) and for $\Gamma = 5/3$ (Lee & Ostriker 1986). They were followed by many other studies using both linear theory (McMillan et al. 1987; Kochanek 1992) and numerical hydrodynamical calculations (Rasio & Shapiro 1991). Such treatments give $R_{\rm p}/R_2$ between 2 and 3 as a condition for tidal capture (the exact value depending on the properties of the stellar structure model used). Thus an approximate condition for tidal capture may be given as $R_{\rm p} \leq 3R_2$ irrespective of the precise details since for $R_{\rm p}/R_2 \leq 3$, $\omega_{\rm p} \sim \omega_{\rm osc}$.

For compact binaries, angular momentum losses to gravitational waves, as well as dynamical mass ejection from the system must additionally be considered. The results for a black hole-neutron star encounter with mass ratio $q = 0.31$, $\eta = 3$ (corresponding to $R_{\rm p}/R_2 = 3.1$),

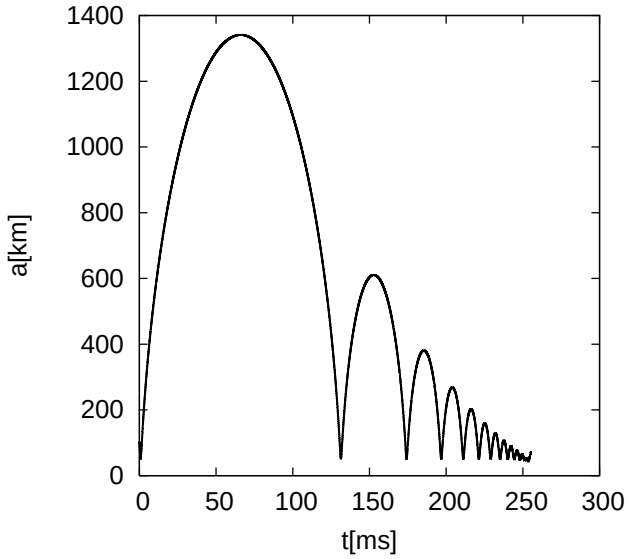

FIG. 1.— The encounter of a neutron star with a black hole at relatively large impact parameter (run L_3) leads to a large number of periastron passages before tidal disruption. Here we show the separation (in km) between the neutron star and the black hole from the start of the simulation until full disruption of the star, taking about one quarter of a second.

TABLE 1
Parameters for orbital encounters.

Run	Prim.	Sec.	Γ	$\frac{M_1}{M_\odot}$	$\frac{M_2}{M_\odot}$	$q=\frac{M_2}{M_1}$	η	$\frac{R_\mathrm{p}}{R_2}$
L_0	BH	NS	2	4.51	1.4	0.31	1.0	1.5
$L_0\Gamma_{5/3}$	BH	NS	5/3	4.51	1.4	0.31	1.0	1.5
L_1	BH	NS	2	4.51	1.4	0.31	1.5	1.9
L_2	BH	NS	2	4.51	1.4	0.31	2.0	2.3
$L_2\Gamma_{5/3}$	BH	NS	5/3	4.51	1.4	0.31	2.0	2.3
L_3	BH	NS	2	4.51	1.4	0.31	3.0	3.1
NSNS	NS	NS	2	1.75	1.4	0.80	1.0	1.0
BHWD	BH	WD	5/3	2.5	0.5	0.20	1.0	1.7

where the neutron star is modeled as a polytrope with $\Gamma = 2$ (run L_3 in Table 1) are shown in Figure 1. As expected, the strong tides trigger complex oscillations in the secondary star which can be clearly seen in the variation of the maximum density in the core after the first periastron passage. Further energy transfer occurs in subsequent passages as the orbit becomes tighter and progressively circular, until eventually some direct mass transfer takes place along with mass stripping. We find that the secondary is not shredded immediately, but only after more than a dozen passages at about the same periastron distance. Our condition for for tidal capture is in rough agreement with $R_\mathrm{p}/R_2 \leq 3$ although the inclusion of gravitational waves as well as matter ejection from the system allows for a more rapid variation of angular momentum disposal. For $\eta \simeq 1$, the secondary star will experience a direct physical collision at least of its outer layers. The process is rather complex with some of the gas escaping entirely from the system on outbound trajectories. The core may preserve its integrity for a few orbital periods around the primary in a *common envelope* before finally coalescing. It is to this problem that we now turn our attention.

A summary of the most important aspects of the initial conditions thus chosen is given in Table 1. There are six parabolic encounters involving neutron stars with black holes, one double neutron star collision, and one black hole–white dwarf encounter. The parameter η has been computed from the point mass orbital parameters in Newtonian gravity. Naturally the centers of mass of each star do not follow these solutions because of finite size effects and the emission of gravitational waves, but they allow for a characterization of each case. Note that since $\eta \propto R_\mathrm{p}^{3/2}$ and $L \propto R_\mathrm{p}^{1/2}$, the change in η by a factor 3 is actually a variation of $3^{1/3} \approx 1.4$ in orbital angular momentum.

2.4. *Stellar disruption and disk formation*

For binary mergers, tidal disruption usually occurs after a single periastron passage, because the system is already very tightly bound by gravity. In the case of collisions, we find that the secondary is not shredded immediately after the first interaction. It does, however, lose a substantial amount of orbital energy and angular momentum through two main channels: emission of gravitational waves and transfer by gravitational torques through the formation of the tidal bulge. The bulge in effect deforms the spherical star into a bar, which the primary can then spin-up during the brief encounter. The strong tides additionally trigger complex, nearly radial

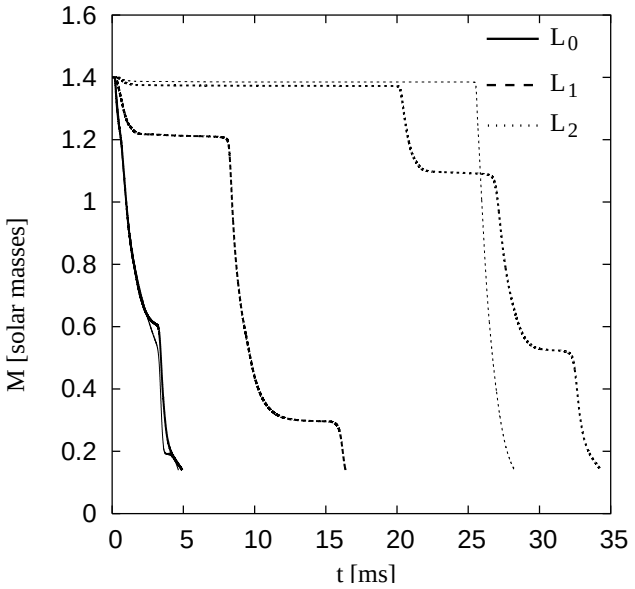

Fig. 2.— The neutron star core mass decreases during the collision with a black hole by tidal mass stripping. As the strength of the encounter, η, decreases, the neutron star survives for a greater number of periastron passages before being eventually shredded. The secondary's mass (in solar masses) is shown for runs L_0, $L_0\Gamma_{5/3}$, L_1, L_2 and $L_2\Gamma_{5/3}$ until disruption. The thick (thin) lines are for $\Gamma = 2$ ($\Gamma = 5/3$).

oscillations in the secondary which can be clearly seen in the variation of the maximum density in the core after periastron passage. Some direct mass transfer occurs as well, along with mass stripping which can form a first accretion structure around the primary, which is more massive for low initial impact parameters. Additionally, some matter is flung out through the exterior Lagrange point to large distances, creating a tidal tail.

In runs L_0 and L_1, the neutron star core (which now contains $\simeq 1\ M_\odot$ and $1.2\ M_\odot$ respectively, see Figure 2) does not survive the second encounter, and forms a massive disk around the black hole, as well as an elongated tidal tail. In run L_2 there is enough energy and angular momentum at the outset that the core is able to return a third time, after which it too is fully disrupted and forms a disk (see Figure 3). Each successive passage feeds the accretion disk and simultaneously forms a tidal tail, which is not set to collide with previous ejections. We show in Figure 4 the time evolution for different initial impact parameters, projected onto the orbital plane. Even with three periastron passages, the collision and disruption are essentially over after $\simeq 50$ ms, because the initial passage drains enough orbital energy and angular momentum to bind the system very effectively.

For runs carried out with a soft equation of state, $\Gamma = 5/3$, the results are qualitatively the same for low impact parameter, with the main difference being in the spatial extent of the accretion disk formed, and in that of the tidal tails, both being greater than for $\Gamma = 2$. For large impact parameter, the gravitational interaction is quantitatively different during the first periastron passage, since the star effectively resembles a point mass to a greater degree in run $L_2\Gamma_{5/3}$. Angular momentum and

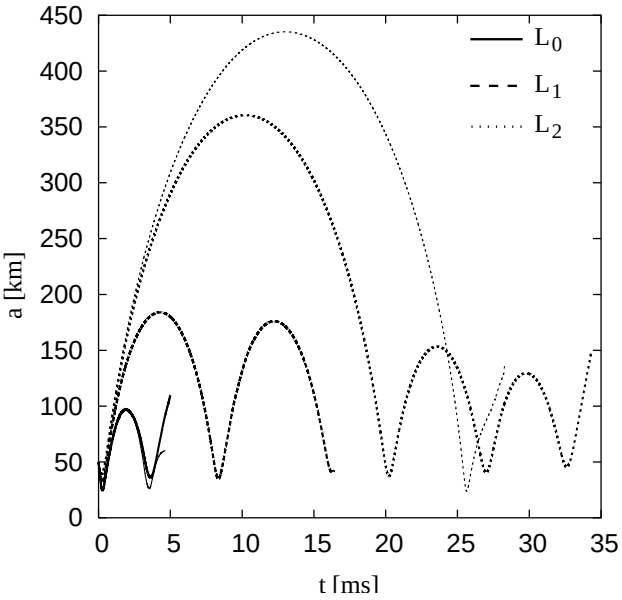

FIG. 3.— The separation (in km) between the neutron star and the black hole is shown until disruption of the neutron star for runs L_0, $L_0\Gamma_{5/3}$, L_1, L_2 and $L_2\Gamma_{5/3}$. Note the change in scale on the time axis when compared with Figure 1. The thick (thin) lines are for $\Gamma = 2$ ($\Gamma = 5/3$).

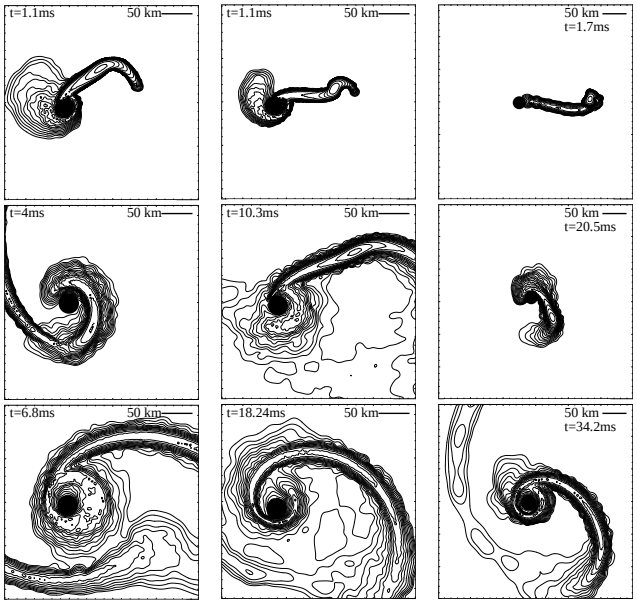

FIG. 4.— Parabolic collisions of neutron stars with black holes. Logarithmic contours of density in the orbital plane (equally spaced every 0.25 dex) are shown for runs L_0 (left), L_1 (middle) and L_2 (right). The lowest contour in bold is at $\log \rho$ [g cm^{-3}] = 10. The time elapsed since the beginning of the simlulation is indicated in each panel (increasing top to bottom), as is the distance scale. Note the different number of periastron passages and tidal tails formed until final disruption in each case.

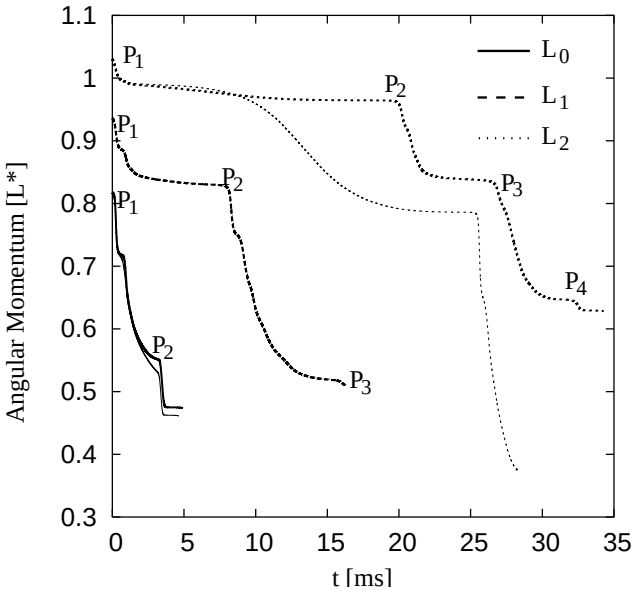

FIG. 5.— The total angular momentum as a function of time is shown for runs L_0, $L_0\Gamma_{5/3}$, L_1, L_2 and $L_2\Gamma_{5/3}$, in units of $L^* = M_{\rm tot}\sqrt{G\mu R_{\rm NS}}$, where $M_{\rm tot}$ is the total mass and μ is the reduced mass. For each case, successive periastron passages are marked on the curve as P_1, P_2, ...The thick (thin) lines are for $\Gamma = 2$ ($\Gamma = 5/3$).

energy transfer through torques is thus less efficient and the core of the neutron star is transferred to a higher orbit than in run L_2 (note the difference in secondary apocenter values in Figure 3). At the secondary passage $\simeq 26$ ms after the start of the simulation, however, the star is fully shredded by tidal forces and the final disk forms promptly.

For the disruption of a star by a *supermassive* black hole, the former moves essentially in the fixed background metric imposed by the hole, and this allows for a simplified treatment of the dynamics. It was found in earlier studies (Rees 1988), both through analytical considerations and direct numerical simulation, that essentially half the mass of the star is dynamically ejected, while the remaining half is captured by the black hole, being on eccentric trajectories which, with variable delay, will bring them back to the vicinity of the primary.

There are two important differences between such a scenario and that considered in the present study. First, as already noted, the mass ratio is of of order 0.1-1 instead of 10^{-7}, which can produce a direct collision with accompanying mass transfer simply by virtue of the small periastron distance of a disruptive event. Second, at the small distance scales implied by the fact that we are considering compact stellar mass objects, gravitational wave emission is intense, and can drain a substantial fraction of the total kinetic energy and angular momentum during a single passage (see Figure 5). Thus the system becomes non-conservative from a point of view of orbital dynamics, and the previous reasoning does not apply.

After the neutron star has been fully disrupted, the remnant consists of a black hole surrounded by a torus, and a series of tidal tails, depending on the number of periastron passages which occurred. The tori are typically

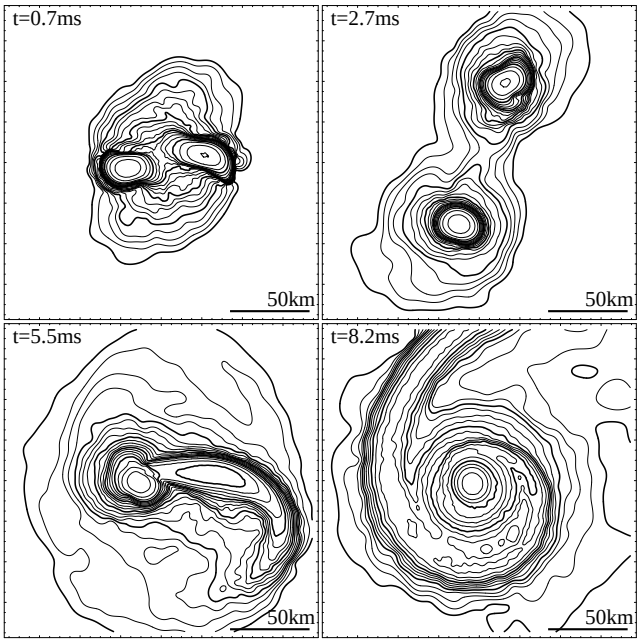

FIG. 6.— Logarithmic contours of density in the orbital plane (equally spaced every 0.25 dex) for the collision of two neutron stars (run NSNS) on a parabolic orbit with initial mass ratio $q = 0.8$. The lowest contour in bold is at $\log \rho$ [g cm^{-3}] = 10. After an initial passage the secondary is entirely disrupted and wraps around the primary, forming an envelope and a single tidal tail.

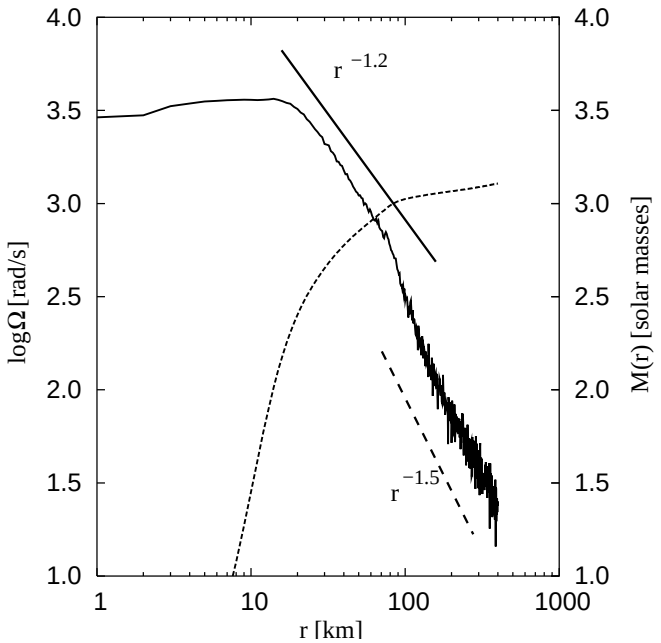

FIG. 7.— Azimuthally averaged angular velocity profile (solid line) and enclosed mass (dashed line) in the double neutron star collision remnant. The rapidly rotating inner core (P=2.1 ms) is surrounded by a large envelope. The rotation of the tidal tail is visible at radii greater than 100 km, and reference power laws are given for the envelope and tail.

200-300 km across and contain $M_{\rm disk} \simeq 0.1 M_\odot$. They are comparable in size and mass to those encountered during binary mergers, with densities $\rho \simeq 10^{11} - 10^{12}$ g cm^{-3} and internal energies $u \simeq 10^{18} - 10^{19}$erg g^{-1}, equivalent to 1-10 MeV/baryon. The binary interaction is violent and complex, though, and this can be qualitatively seen in the fact that by the end of our calculations (roughly 20 ms) the accretion structures still show significant deviations from azimuthal symmetry.

For double neutron star encounters, the mass ratio is even greater (we have computed one collision for $q = 0.8$, which is likely to be a lower bound for such systems). For the case considered with adiabatic index $\Gamma = 2$, the two stars are actually the same size, and directly impact each other for an encounter strength $\eta = 1$. The initial collision binds the stars in an elliptical orbit but does not lead to the formation of a significant tidal tail. The less massive secondary is strongly distorted and spun up, and a bridge of material temporarily joins the two stars. Upon a second passage the secondary is entirely shredded and wraps around the primary (see Figure 6). The material from each stars remains largely separate, with that from the primary remaining essentially in the core, in a manner similar to what is obtained for mergers of unequal mass neutron stars.

The final remnant in this case consists of a slightly differentially rotating core of $2.4 M_\odot$ with radius $R_{\rm core} \simeq$ 20 km and a maximal rotation frequency of $\Omega_{\rm max} \simeq$ 3000 rad/s, corresponding to a period of 2.1 ms (see Figure 7). This is surrounded by an envelope out to $\sim$ 80 km containing $M_{\rm env} \simeq 0.49 M_\odot$, where the orbital frequency is $\Omega \propto r^{-1.2}$. In the outer tail of material the rotation is essentially Keplerian, with $\Omega \propto r^{-1.5}$ (the rotation profile is shown as well in Figure 7). Note that the core is above the threshold for collapse of a cold, non–rotating configuration in most equations of state, but could avoid this given the rapid and differential rotation present (Cook et al. 1994; Baumgarte et al. 2000). In addition significant heating of the core can raise the critical threshold mass for collapse to $\simeq 1.35 M_{\rm cold}$ (Shibata & Taniguchi 2006). In this particular case the core could conceivably remain stable for a longer time, spinning down on a secular time scale due to the emission of gravitational waves or magnetic torques. If it were to indeed form a black hole, the distribution of angular momentum in the envelope is such that only material between 50 and 100 km, amounting to $0.17 M_\odot$, would have enough centrifugal support to form an accretion disk.

For completeness we have also considered the interaction of a low mass ($M_{\rm WD} = 0.5 M_\odot$) white dwarf with a compact object ($M_{\rm co} = 2 M_\odot$). The latter could be either a massive neutron star or a low mass black hole. Numerically it is irrelevant because the characteristic scales of the two objects are so different that it is impossible to resolve simultaneously the black hole horizon (or neutron star surface) and the entire white dwarf. For the actual calculation the absorbing accretion boundary has been placed 100 gravitational radii from the center of the compact object.

The white dwarf is modeled as a polytrope with adiabatic index $\Gamma = 5/3$, appropriate for a cold, non-relativistic degenerate configuration, and the pressure is thus given by $P = K_{\rm n.r.} \rho^{5/3}$, where $K_{\rm n.r.} = (3/\pi)^{2/3} h^2 / (20 m_e (2 m_p)^{5/3})$. With the given mass, the stellar radius is $R_{\rm WD} = 1.1 \times 10^9$ cm, a factor $f \simeq 800$ larger than our standard neutron star. In fact with the same input physics one could simply scale the results from the BH-NS interaction (given an identical mass ratio) by increasing distances by a factor f and temporal

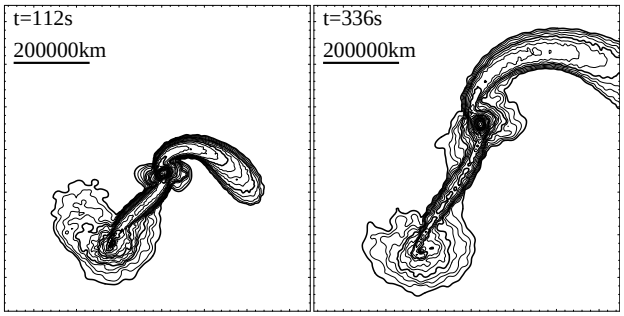

FIG. 8.— Logarithmic density contours (equally spaced every 0.25 dex) for the encounter between a low mass white dwarf and a compact object. The lowest contour in bold is at $\log \rho$ [g cm^{-3}] = 3. Note the difference in scales (spatial and temporal) when compared to those in Figures 4 and 6. The higher compressibility of the material also makes for a wider distribution of ejected material and a generally wider distribution of gas.

TABLE 2
DISK, TAIL AND EJECTED MASSES.

Run	$M_{\rm disk}/M_\odot$	$M_{\rm tail}/M_\odot$	$M_{\rm ej.}/M_\odot$
L_0	0.23	0.15	0.05
$L_0\Gamma_{5/3}$	0.25	0.11	0.04
L_1	0.16	0.31	0.13
L_2	0.09	0.47	0.19
$L_2\Gamma_{5/3}$	0.11	0.19	0.04
NSNS	0.17	0.13	0.03
BHWD	0.13	0.35	0.24

scales by $f^{3/2} \simeq 2.3 \times 10^4$ (giving hundreds of seconds instead of tens of milliseconds). This is strictly not correct, however, since gravitational radiation reaction introduces an absolute scale into the problem, and energy and angular momentum losses through this channel are insignificant in comparison to the BH-NS case. The interaction proceeds then at a more leisurely pace, so much so that we were unable to follow it to a second periastron passage, even though the simulation covered nearly one thousand seconds. At this stage stripping during the close passage has formed a torus around the compact object, linked to the stellar core by a long and narrow bridge of material (see Figure 8). The core itself is rapidly spinning due to gravitational torques exerted by the primary, and the typical tidal tail has formed at large radii.

Since we are considering encounters in which disruption occurs practically by construction (given the choice of the parameter η), the gravitational torques exerted on the secondary are of comparable magnitude in all cases (with appropriate scalings). We find that the angular frequency of the core after the first periastron passage is $\simeq (0.2-0.4)\Omega_0$, where $\Omega_0 = (GM_2/R_2^3)^{1/2}$ is the break up rotation frequency of the unperturbed secondary. Thus the spin periods are $\simeq 2$ ms and $\simeq 8$ s for encounters involving neutron stars and white dwarfs respectively.

The mass of the disk (see Table 2) present at the end of the calculation as a result of the encounter is computed from the fluid elements in close, essentially circular orbit about the central object. It is typically $M_{\rm disk} \simeq (0.1-0.3)M_\odot$, regardless of the type of encounter. Likewise, the mass of the tidal tails, $M_{\rm tail}$, is obtained by adding over all the fluid elements within these structures, whether they are bound to the central mass or not. For black hole-neutron star encounters there is a clear trend of decreasing disk mass and increasing tail mass as the initial impact parameter grows at fixed compressibility. The total amount of matter dynamically ejected (computed as that with positive total energy) also increases, and is a result of the greater number of ejection episodes associated with larger values of the orbital angular momentum. For run L_2 we find that nearly $0.2M_\odot$ are thus lost. For the double neutron star collision the characteristics of the system (total mass and mass ratio) are such that the ejected mass is significantly lower, although a substantial tail is still present. We will return to the implications of mass ejection below. Including the effects of General Relativity will likely alter these values, by up to one order of magnitude if the differences between calculations performed in Newtonian theory and those using GR for mergers are used as guidance.

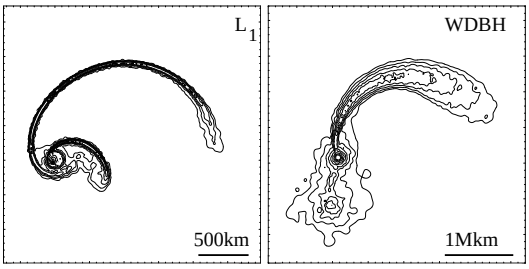

FIG. 9.— Tidal tails formed by the disruption of a neutron star by a black hole (run L_1) and a white dwarf (run WDBH). For the neutron star disruption the impact parameter was such that two periastron passages occurred, giving rise to two distinct ejection structures thousands of kilometers across by the end of the simulation. For the case involving the white dwarf, only one passage has occurred and the core of the star is still present. Note the much larger spread in the distribution of the fluid, due to the lower adiabatic index used in the case of the white dwarf.

2.5. *Tidal tails and mass ejection*

For the two members of the system to come together and eventually merge, they must lose energy and angular momentum. This can be achieved through the emission of gravitational waves, or the ejection of matter, or a combination of both. In either a binary system in circular orbit or a parabolic approach there is a substantial amount of rotation. Since a small amount of matter, removed to a large radius, can carry a great deal of angular momentum, the formation of tidal tails out of material stripped through the outer Lagrange points in the effective potential is an efficient way to produce a single object at the center. This is the fundamental reason why such structures form in either stellar or galactic collisions.

Just as the vanishing orbital energy of a parabolic orbit implies successive periastron passages as the core becomes more and more bound to the primary, so too it is easier to dynamically unbind matter to infinity when compared to a bound binary. As each passage proceeds a new ejection episode occurs, giving rise to an additional tail (Figure 9). The amount of mass thus ejected, and shown in Table 2, is considerably greater than for a binary coalescence, by about one order of magnitude (Lee 2001).

In all cases when multiple ejection events occur (we observed up to three for run L_2), the velocities and orien-

tations are such that the initial tail will not be overtaken by latter ones. This is simply because the first one has a clear head start, but also because subsequent events occur at different orbital phases.

An interesting point regarding the tails concerns their hydrodynamic stability. Their motion is essentially ballistic, dominated by the potential well of the central mass. They are nevertheless susceptible to the varicose, or sausage instability first identified by Rayleigh in 1899 (Chandrasekhar 1961). This is due to self-gravity and occurs for cylindrical configurations of an incompressible fluid for perturbations with wavelength $\lambda > \lambda^* = 2\pi R_{\rm cyl}/x^*$, where $x^* \simeq 1$ and $R_{\rm cyl}$ is the radius of the cylinder. The fastest growing mode has $x = 0.58$, wavelength $\lambda \simeq 11 R_{\rm cyl}$ and a growth time $\tau = 4/(4\pi G\rho)^{1/2}$ (Chandrasekhar 1961). For sufficiently stiff equations of state (with adiabatic index $\Gamma > 2.5$), even though not strictly incompressible, this is actually seen in numerical simulations (Rasio & Shapiro 1994; Lee 2000): on a time scale given approximately by τ, condensations form, and are separated roughly by the wavelength of the fastest growing mode given above. For softer equations of state (even such as the one used here for neutron stars when $\Gamma = 2$) the effect is not present, and even less so for the calculation involving the neutron star with $\Gamma = 5/3$ and the white dwarf (Figure 9).

3. EMISSION OF GRAVITATIONAL WAVES

In the case of merging binaries, the early gravitational waveforms, when the separation is much larger than the stellar radius, can be computed using the weak field approximation analytically, and from them the stellar masses may be accurately determined. As the stars become distorted by the tidal field, the signal deviates form this solution and finite size effects accelerate the decay. The secondary is then fully accreted by the black hole (if one is present) or tidally disrupted, and the emission abruptly ceases. The precise frequency where this occurs can lead in principle to accurate determinations of the neutron star radius (Faber et al. 2002), and thus, since the mass is already known, to useful constraints on the equation of state at supra-nuclear densities.

The total mass and relative velocities involved in a parabolic encounter are similar to those encountered in close binaries, and so we would expect the characteristic frequencies and strength, or amplitude of the signal in gravitational waves, to be comparable in this case. The biggest difference arises, and is crucial in terms of detectability, because the collision does not involve a leisurely spiral in over many orbital periods, and as thus lacks the characteristic precursor chirp signal which would slowly sweep through the interferometer's detection band. Figure 10 shows the computed waveforms (one polarization is given) for black hole-neutron star encounters and the double neutron star collision.

A neutron star (M_2) approaching a stellar mass black hole (M_1) with $\eta \sim 1$ will be disrupted in a single passage and the particles in the disrupted remnant follow approximately independent Keplerian orbits. The detectable gravitational signal will thus have a burst-like

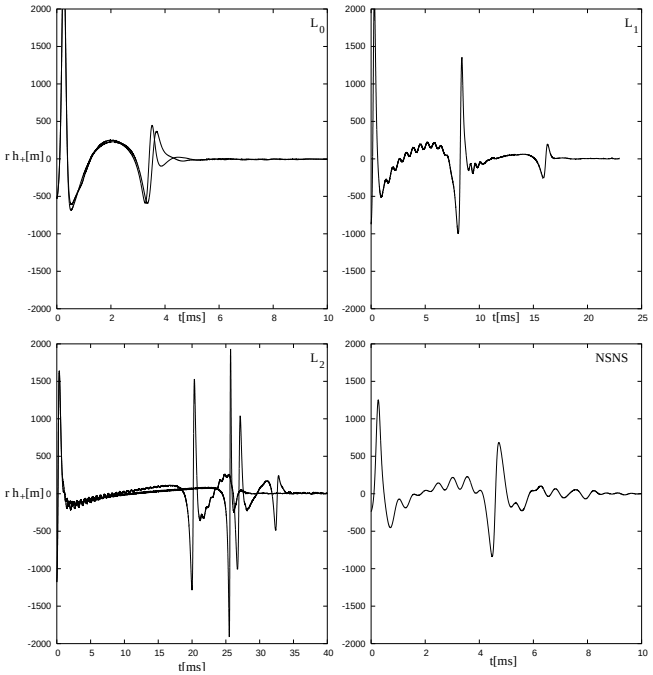

FIG. 10.— Gravitational waves emitted as a function of time for runs L_0, $L_0\Gamma_{5/3}$, L_1, L_2, $L_2\Gamma_{5/3}$, and NSNS as seen by an observer placed along the rotation axis (rh_+ is plotted (in m), where r is the distance from the source to the observer). The thick (thin) lines are for $\Gamma = 2$ ($\Gamma = 5/3$). The vertical range is identical in all frames, but note the different scaling on the time axis. In all runs except for L_0, $L_0\Gamma_{5/3}$, and $L_2\Gamma_{5/3}$, the oscillations of the neutron star core following the first and even second periastron passage are clearly visible. When varying the stiffness of the equation of state, the waveforms are nearly indistinguishable for small impact parameter and clearly separated for large values, due to the difference in the associated orbital evolution.

behaviour, roughly characterized by an amplitude

$$h \sim \frac{GMR_1}{c^2 D R_{\rm p}} \sim 10^{-22}\,\eta^{-2/3}\left(\frac{D}{100\,{\rm Mpc}}\right)^{-1} \times \left(\frac{M_1}{10\,M_\odot}\right)^{2/3}\left(\frac{R_2}{10\,{\rm km}}\right)^{-1}\left(\frac{M_2}{1.4\,M_\odot}\right)^{4/3}, \quad (4)$$

and frequency

$$f \sim \left(\frac{GM_1}{R_p^3}\right)^{1/2} \sim 1.4\times 10^4\,{\rm Hz}\times \eta^{-1}\left(\frac{R_2}{10\,{\rm km}}\right)^{-3/2}\left(\frac{M_2}{1.4\,M_\odot}\right)^{1/2}. \quad (5)$$

Here M denotes the total mass, $M_1 + M_2$. LIGO will be able to detect gravitational wave from impact involving neutron stars and stellar mass black holes if $\eta \leq 1$ and the distance is $D \leq 50$ Mpc. In what follows, we compare these simple estimates of gravitational radiation against more detailed results obtained with our numerical scheme.

The signal exhibits a local peak at each periastron passage, until the time when the star is completely disrupted and the amplitude vanishes (note the different time scales on each plot in Figure 10). In runs L_1, L_2 and NSNS, smaller oscillations of decaying amplitude after each passage (but perhaps the last) are also clearly present when

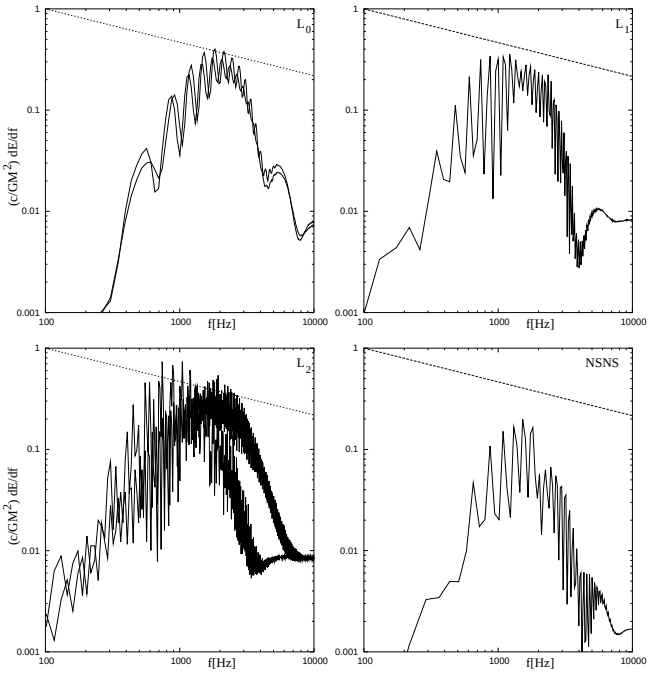

FIG. 11.— Gravitational wave energy spectrum for runs L_0, $L_0\Gamma_{5/3}$, L_1, L_2, $L_2\Gamma_{5/3}$ and NSNS. The ranges are identical in all frames. The reference power law is $dE/df \propto f^{-1/3}$, the characteristic spectrum for the in-spiral of a point mass binary. The thick (thin) lines are for $\Gamma = 2$ ($\Gamma = 5/3$). The oscillating nature of these spectra is due to the finite extent of wave trains present in the amplitudes during different segments of temporal evolution.

$\Gamma = 2$. For instance, for run L_2 between 3 and 15 ms, their frequency is $\nu_{\rm osc} \simeq 1750$ Hz. This is *not* due to the rotation of the neutron star (the spin frequency of the core is at this point approximately $\nu_{\rm spin} \simeq 320$ Hz) but essentially to radial vibration modes excited by the action of the primary at periastron passage. The frequency of such modes is close to the natural value given by hydrostatic equilibrium, namely $\nu_{\rm osc} \simeq (GM/R^3)^{1/2}/2\pi \simeq 1400$ Hz. The small impact parameter and rapid disruption of the star in run L_0, and the high compressibility used in run $L_2\Gamma_{5/3}$ does not allow for a clear manifestation of such oscillations.

The power spectrum of these gravitational waves is shown in Figure 11. There are peaks at 1900, 1600 and 1000 Hz for runs L_0, L_1 and L_2, respectively. These correspond to the interaction time for each run, which increases (thus decreasing the frequency) as the impact parameter (or equivalently, the total angular momentum in the system) increases. Secondary periastron passages make this peak wider at higher frequencies. This is particularly evident when comparing the results of runs L_2 and $L_2\Gamma_{5/3}$. The latter has a single late-time periastron passage (instead of three for the former), and the peak is broadened to $\simeq 2000 - 3000$ Hz. We note that the oscillation frequency of the core, visible in the signal when $\Gamma = 2$, is undetectable in these spectra, being buried within the main peak due to the binary interaction (this is to be expected, since by definition of a tidally disruptive event, the interaction time is roughly equal to the free fall time scale of the star). The spectrum for run NSNS shows a similar overall structure. We note that it is difficult to extract a clean spectral signal with a high signal to noise ratio, because the simulated time is quite limited. Secondary high frequency variations at $\simeq 5000$ Hz can be seen in the spectra for runs L_0, L_1 and NSNS and are related to the asymmetry of the waveform around the time of closest approach. The large number of periastron passages in run L_2 makes the spectrum more noisy and this feature is not observed. Finally, we also show the gravitational wave luminosity in Figure 12, the integration of which reveals that the efficiency for their emission is $\epsilon = E_{\rm GW}/(Mc^2) = 10^{-2}, 7\times10^{-3}, 6.8\times10^{-3}, 5.9\times10^{-3}$ for runs L_0, L_1, L_2 and NSNS respectively. For comparison, the efficiency in the case of a merging binary with the same mass ratio is $\approx 5\times10^{-3}$ (Lee 2001). We note also from Figure 12 that the maximum power radiated during a collision and even during subsequent close approaches can be significantly higher than that in a merging binary with the same mass ratio, due to the larger velocities in an eccentric orbit at periastron.

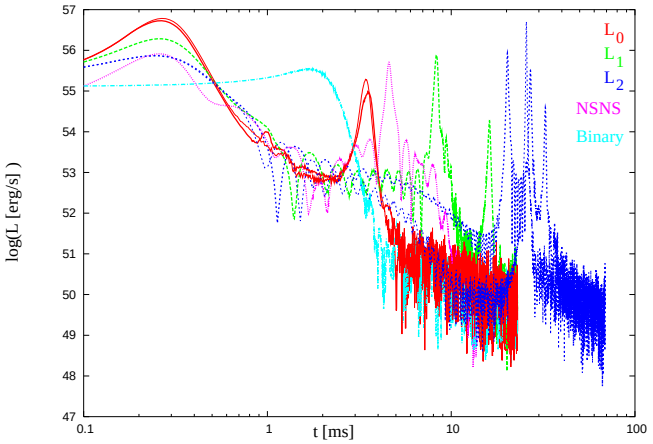

FIG. 12.— Power radiated in gravitational waves for black hole-neutron star encounters and the double neutron star collision. There is one successively weaker peak for each periastron passage until complete tidal disruption. The curve labeled "Binary" shows the luminosity computed for a black hole-neutron star binary with the same mass ratio, $q = 0.31$ and initial separation, $r_i = 3.7R_{\rm NS}$, as runs L_0 through L_2, for which disruption occurs promptly after the beginning of mass transfer (Lee 2001). The thick (thin) lines are for $\Gamma = 2$ ($\Gamma = 5/3$). When varying the stiffness of the equation of state, the luminosities are nearly indistinguishable for small impact parameter and clearly separated for large values, due to the difference in the associated orbital evolution.

4. THE RATES OF COLLISIONS AND TIDAL CAPTURES OF COMPACT OBJECTS IN GLOBULAR CLUSTERS

The highest stellar densities in GCs are reached in the core, in particular during core collapse. In this section we estimate the collision and tidal capture rate as a function of time by first reconstructing the core evolution of a typical post-core-collapse GC. We then re-scale the resulting encounter rate evolution with the measured mass and size distribution of GCs in galaxies to obtain the rate per host galaxy. Finally, for a given galaxy luminosity density distribution, we obtain per volume of space and as function of time, the expected global rate of collisions and tidal capture of compact objects in the cores of GCs. The details of the encounter rate calculation will be presented in an forthcoming paper (van de Ven et al., in prep.), of which we give here a summary focussing on close encounters between compact stars.

4.1. *Close encounters*

TABLE 3
Relative encounter rates.

type 1	type 2	$M_2/\mathrm{M}_\odot$	R_2/km	$\xi_{\rm col}$	$\nu_{\rm tid}/\nu_{\rm col}$	$R_{\rm min}/R_2$
NS	NS	1.4	10	1.00	6.68	13.37
BH	BH	4.5	13	4.18	6.80	13.60
WD	WD	0.5	11000	392.87	2.99	5.99
BH	NS	-	-	4.85	7.18	16.51
NS	WD	-	-	747.11	7.12	7.12
BH	WD	-	-	1966.61	10.03	10.04

We assume the different types of stellar objects, i, are distributed homogeneously within a spherical core of radius $r_{\rm c}$, each with fractional number $f_i \leq 1$ and total number density $n_{\rm c}$. We further assume that the stars follow a Maxwellian velocity distribution function with dispersion $\sigma_{\rm c}$. Together with the dominating gravitational focusing, this means we can approximate (Heggie 1975) the total collision rate as

$$\nu_{\rm col} = 2.1\times10^{-3}\,\mathrm{Gyr}^{-1}\,\frac{f_1\,f_2}{1+\delta_{12}}\times \left(\frac{n_c}{10^6\,\mathrm{pc}^{-3}}\right)^2\left(\frac{r_c}{0.1\,\mathrm{pc}}\right)^3\left(\frac{\sigma_c}{10\,\mathrm{km\,s}^{-1}}\right)^{-1}\times \left(\frac{M_1+M_2}{1\,\mathrm{M}_\odot}\right)\left(\frac{R_{\rm min}}{10\,\mathrm{km}}\right), \quad (6)$$

where $\delta_{12}=1$ if type 1 and 2 are equal, and $\delta_{12}=0$ otherwise. The stars have masses M_i, and their separation at closest approach is given by $R_{\rm min}$, which we take to be the sum of the stellar radii, i.e., $R_{\rm min}=R_1+R_2$.

In addition, we also consider encounters in which stars pass close enough to each other to form a binary by transfering orbital energy to internal stellar oscillations. We adopt a cross section for tidal capture of the form (Lee & Ostriker 1986)

$$\Sigma_{\rm tid} = a\left(\frac{v_{\rm inf}}{v_{\star,2}}\right)^{-\beta} R_2^2, \quad (7)$$

where $v_{\rm inf}$ is the relative velocity at infinity, and $v_{\star,2}=(2GM_2/R_2)^{1/2}$ is the escape velocity at the surface of the secondary, captured star. We use the fitting functions of Kim & Lee (1999) to obtain the amplitude a for encounters between different stellar types, while the slope $\beta\simeq2.2$ in all cases. In case of collisions dominated by gravitational focussing, the cross section is of the same form, but with slope $\beta=2$. Henceforth, we can express the tidal capture rate $\nu_{\rm tid}$ in the same way as the collision rate in equation (6), but with closest approach given by

$$R_{\rm min} = \Gamma(2-\beta/2)\frac{a}{\pi}\frac{M_2}{M_1+M_2}\left(\frac{2\sigma_{\rm c}}{v_{\star,2}}\right)^{2-\beta} R_2, \quad (8)$$

where Γ is the complete gamma function.

In what follows, we focus on the collision and tidal capture rate between two neutron stars. Since we assume a homogeneous distribution of stars in the core, these results can be re-scaled for close encounters between other types of stellar objects. In Table 3, we give these scaling factors in case of a neutron star (NS), a stellar black hole (BH), and a white dwarf (WD), with (typical) masses and radii as indicated. After taking into account the relative differences in fractional numbers f_i, the collision rate follows from multiplying the (default) NS-NS collision rate by the factor $\xi_{\rm col}$ in column 5. In turn, multiplying the resulting collision rate with the factor in column 6 yields an estimate of the tidal capture rate. Here we neglect the weak dependence of $R_{\rm min}$ in equation (8) on $\sigma_{\rm c}$, which in turn varies only mildly during the evolution of the core. While in general a tidal capture does not necessarily lead to the coalescence of the two stellar objects (Lee & Ostriker 1986), in case of compact objects the approach is so close (see $R_{\rm min}/R_2$ in column 7) that they will merge well within a Hubble time. In particular, for two neutron stars the close encounter rate is boosted by a factor $\simeq 6.7$ due to tidal capture, without any significant delay with respect to collisions because of the very efficient emission of gravitational waves.

The encounter rate might be significantly enhanced due to interactions between single stars and stellar binaries (and even between binaries), which have a much larger cross section, with $R_{\rm min}$ proportional to the binary separation. Moreover, due to mass segregation the more massive stellar objects, including binaries, sink towards the center and can be important or even dominant in the core. Still, only the stars in very "hard" binaries with small enough separations (and thus smaller cross sections) might coalesce within a Hubble time. We discuss binaries in Section 4.5 below, in particular focussing on compact binaries as they are commonly believed to be the progenitors of SGRBs. We restrict however the encounter rate calculations to collisions and tidal captures between single stars, and hence consider the resulting values as lower limits.

4.2. *Evolving encouter rate*

After gradual contraction during an early phase, the core of a GC can go into deep self-similar collapse (Lynden-Bell & Eggleton 1980). The collapse is halted due to engery release from interactions with binaries, also known as binary burning (Hills 1975), and/or from other sources including a possible intermediate-mass black hole (Shapiro 1977). The post-collapse evolution has been extensively studied (see e.g. Heggie & Ramamani 1989), but many aspects are still intensively investigated and debated. For example, Fregeau (2008) recently proposed that the observed post-core-collapse GCs ($\simeq$ 20 % in the Milky Way) are most likely in the binary burning phase, while the remaining GCs are still in the process of core contraction and have not yet reached the binary burning phase. In the meantime, matching Monte Carlo models of M 4 (Heggie & Giersz 2008) and of NGC 6397 (Giersz & Heggie 2009) seem to reveal that both GCs are past collapse in the binary burning phase, even though only NGC 6397 is one of the observed post-core-collapse GCs, while the surface brightness of M 4 is well fitted by a standard King profile. Giersz & Heggie (2009) argue that the differences in the surface brightness profiles are most likely due to fluctuations in the core after collapse. They point out that it is well possible that most GCs are post-core-collapse, but only a fraction happens to be at the "peak" of the fluctuations that corresponds to a cusped surface brightness profile and leads to post-core-collapse classification. These fluctuations are not necessarily the well-known gravothermal oscillations (Bettwieser & Sugimoto 1984; Goodman 1987), but could be the result of the stochastic nature of binary

burning.

Even though it is clear that the details of these fluctuations are far from known (but see Heggie & Giersz 2009), the core after collapse is expected to be *on average* larger than those of the observed post-core-collapse GCs, and to increase over time to explain the overall dimming in the central surface brightness (see also Fig. 10 of Giersz & Heggie 2009). To mimick this average behaviour, we assume a gradually expanding core after deepest core collapse, which in turn we describe by two classifcal self-similar solutions in two phases. In the early phase expansion mirrors the self-similar late phase collapse, but at a slower rate (Inagaki & Lynden-Bell 1983). After a time since deepest collapse roughly equal to the duration of the late phase collapse (Heggie 1985), the core enters the late phase in which it follows the self-similar expansion of an isolated system (Hénon 1965). We derive the encounter rate during all four phases of collapse and expansion.

In addition to this core evolution model with gradual core expansion after deepest collapse, we also consider a model in which the core properties are kept fixed after deepest collapse. Since the latter "halt of collapse" would mimick binary burning without fluctuations, it provides an upper limit to the contribution of high-density cores, and hence an upper limit to the encounter rate. On the other hand, while the core expansion is just an average approximation to the possible complex fluctuations after deepest collapse, we believe it to provide a closer estimate to the encounter rate. Moreover, we find below (see also Figure 14) that the predicted fraction of (post-)core-collapse GCs is similar to that observed for the MW. The core expansion could also naturally explain why only loose GCs have a shallow/depleted global mass function (De Marchi et al. 2007).

We adopt M 15 as a proto-typical GC that underwent core collapse. Because this GC has been extensively studied and modelled (Dull et al. 1997; McNamara, Harrison & Baumgardt 2004; van den Bosch et al. 2006), its current properties are known accurately. Given the high concentration $c = \log(r_c/r_t) \gtrsim 3$, where r_t is the tidal radius, we assume that the core of M 15 is currently still very close to deepest collapse. The fraction of its age $t_{\rm age} \simeq 13.2\,{\rm Gyr}$ (Baumgardt et al. 2003) that M 15 spent in the early and late phase of core collapse depends on its initial concentration $c_{\rm ini}$. The latter can be inferred from evolved (single-mass) Fokker-Planck models (Quinlan 1996) for a given initial half-mass relaxation time $t_{\rm rh}(0)$. In turn, the latter follows from the current half-mass relaxation time $t_{\rm rh} \simeq 1.42\,{\rm Gyr}$ as $t_{\rm rh}(0) \simeq t_{\rm rh}(t_{\rm age}) - t_{\rm age}/\xi_{\rm dis}$, under the assumption of a constant mass loss rate from the GC (e.g. Vesperini & Heggie 1997). Since the rate of dissolution, $\xi_{\rm dis}$, depends again on the initial concentration (Gnedin et al. 1999), we have to find $c_{\rm ini}$ iteratively.

Doing this, we infer for M 15 $\xi_{\rm dis} \simeq 51$, $t_{\rm rh}(0) \simeq 1.68\,{\rm Gyr}$, and corresponding $c_{\rm ini} \simeq 1.70$. This implies that M 15 spent about 8.0 Gyr in the early phase, and took another 5.2 Gyr to reach the current phase of deep core collapse. Even though the encounter rate during the late phase is expected to dominate over the encounter rate during the early phase, we still take the increase in $\nu_{\rm enc}$ during the early phase into account. In particular,

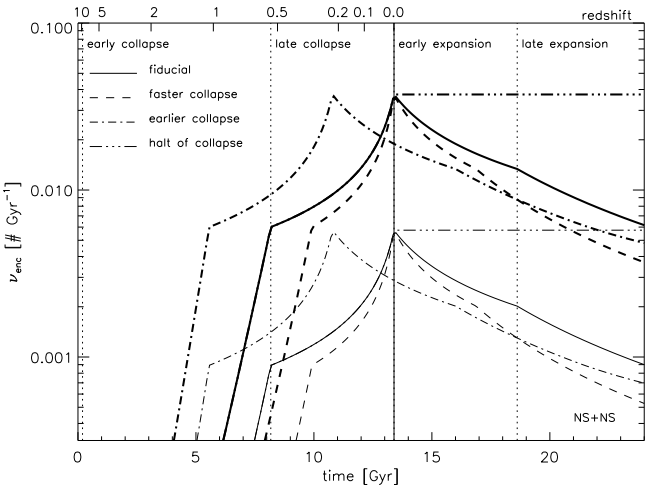

FIG. 13.— An estimate of the encounter rate between two neutron stars in M 15 as function of time (or redshift at the top). The thin lower curves show the predictions for the collision rates, while the thick upper curves present the tidal capture rates. The solid curves are for the fiducial core evolution model, whereas the dashed curves assumes a faster collapse (and expansion), and the dash-dotted curves indicate the effect of an earlier collapse. The dash-triple-dotted curve shows an additional model in which the core properties are kept fixed after deepest collapse. (See Sections 4.2 and 4.4 for further details.)

we take into account the changes in the fractions of stellar types due to mass segregation in the early phase, whereas we assume the fractions to remain constant during deep collapse. We predict the core expansion by mirroring the late phase collapse but with an expansion rate that is a factor 3 slower than the collapse rate. After about 5.2 Gyr (the duration of the late phase collapse) in the future, we expect the core of M 15 to go into the late self-similar expansion phase.

Figure 13 presents the resulting rates as function of time (and redshift along the top axis) for close encounters between two neutron stars in the core of M 15. The number fraction of neutron stars in the core at the beginning of the early phase is less than 1%, but it rises due to mass segregation to about 55% during the self-similar deep collapse (Dull et al. 1997). The thin lower curves show the predictions for the collision rates, while the upper thick curves present the tidal capture rates. The solid curves are for the fiducial core evolution model, whereas the dashed curves assumes a faster collapse (and expansion), and the dash-dotted curves indicate the effect of an earlier collapse. These two variations on the fiducial model are further discussed in Section 4.4 below. Finally, the dash-triple-dotted curve shows the additional model in which the core properties are kept fixed after deepest collapse.

4.3. *Average encounter rate*

We compute an average encounter rate per host galaxy by assuming that all GCs follow an evolution similar to that of M 15, with a scaling in time, based on the half-mass relaxation time $t_{\rm rh} \propto r_h^{3/2} M^{1/2}$. We adopt the distribution in half-mass radii r_h of GCs derived by Jordán et al. (2005), which is independent from the distribution in their total masses M (McLaughlin 2000). It is believed that initially the GC mass distribution followed a power-law, but that especially the less-massive

GCs dissolved, most, if not all, before going into core collapse (McLaughlin & Fall 2008). Hence, we adopt the current GC mass distribution, which is well described by a lognormal distribution (Jordán et al. 2006). After randomnly drawing from these distributions in r_h and M, we arrive at a current half-mass relaxation time, i.e., after a time $t_{\rm age} \simeq 13\,{\rm Gyr}$ since the formation of an average old GC. Adopting the same initial concentration $c_{\rm ini} = 1.70$ as estimated for M 15, we infer the corresponding initial half-mass relaxation time, which we use to re-scale the above derived encounter rate evolution for M 15.

The current and initial half-mass relaxation distributions are shown as solid and dotted histograms in the left panel of Figure 14, while the vertical lines indicate the corresponding values for M 15. Since M 15 has a larger than average half-mass relaxation time, we expect that currently more than half of all GCs are already past reaching deepest core collapse. This is confirmed by the thin solid curve in the right panel of Figure 14, showing the fraction of GCs that past reaching deepest core collapse as function of time. In this fiducial core evolution model it is likely that some time after deepest core collapse the GCs are not anymore *observed* to be post-core-collapse because the core is expanding. Henceforth, to estimate the fraction of observed post-core-collapse GCs, we only count at a given time GCs that are in the late collapse or early expansion phase when the core is smaller. The resulting thick curves show that for the first three models the current fraction (vertical solid line) is similar to the fraction of $\simeq 20\,\%$ of post-core-collapse GCs observed in the Milky Way. Only the halt-of-collapse model predicts a much higher fraction because the core properties are held fixed after deepest collapse.

The number of GCs for which we re-scale the encounter rate evolution of M 15 depends strongly on the total luminosity $L_{\rm gal}$ of the host galaxy (McLaughlin 1999). In Figure 15 we plot the combined encounter rate for a typical $L\star$ galaxy with about a thousand GCs, as well as for a galaxy that is a factor 5 less and more luminous with the number of GCs comparable to that in the Milky Way and in a giant elliptical galaxy, respectively. In the latter two cases we show only the tidal capture rates for the fiducial model, wheras for the $L\star$ galaxy we also indicate the effect of a faster and earlier collapse as discussed in Section 4.4, as well as the additional half-of-collapse model. The results for the collision rate are not shown for clarity, but are similar except for a factor $\simeq 6.7$ decrease in amplitude. In all cases, the encounter rate increases strongly up to redshift $z \sim 1$, but slowly decreases again toward $z = 0$.

Next, we estimate a global encounter rate by combining the previously derived encounter rates per host galaxy with the galaxy luminosity density distribution. The latter is well described by the Schechter function

$$\Phi_{\rm gal}(L) = (\Phi_{\rm gal}\star/L\star)\,(L/L\star)^{\alpha}\exp(-L/L\star), \qquad (9)$$

with $\Phi_{\rm gal\star} = 3.77\times10^{-3}\,{\rm Mpc}^{-3}$ and $\alpha = -1.30$ (Faber et al. 2007). Since the above estimate of the combined encounter rate evolution depends on the *current* luminosity of the host galaxy, the evolution of $\Phi_{\rm gal}(L)$ is not needed to compute the global encounter rate as function of time. However, the latter evolution should be taken into account when discussing the properties of host galaxies, which do change significantly with redshift (see Section 5.3).

In Figure 16, we present our prediction for the global encounter rate $R_{\rm enc}$ (in ${\rm yr}^{-1}\,{\rm Gpc}^{-3}$) between two neutron stars in the core of GCs. The rates both of collisions (thin curves) and of tidal captures (thick curves) show a clear increase around $z \sim 1$, followed by a gradual decline. The tidal capture rate for the fiducial model (thick solid curve) peaks around $z \simeq 0.7$, at a value of $R_{\rm enc} \simeq 55\,{\rm yr}^{-1}\,{\rm Gpc}^{-3}$. This value is fully consistent with the estimated event rates for SRGBs, which are of the order 8–30 ${\rm yr}^{-1}\,{\rm Gpc}^{-3}$ for isotropic radiation (Guetta & Piran 2006). Collimated radiation with opening angles of 30–60°, would boost up the event rates of SGRBs to our predicted global encounter rates. However, since the latter are likely to be rather conservative, smaller opening angles would still be possible.

4.4. *Faster and ealier collapse*

To infer the initial concentration of M15 and the corresponding time spent in the early and late phase of collapse, we used the results of a series of cluster models with single-mass stars (Quinlan 1996). Several complicating factors in real clusters can change the rate of collapse (see e.g. review by Chernoff 1993): for example stellar evolution and especially the presence of primordial binaries slow down the collapse, while mass loss from a tidal boundary and in particular mass segregation accelerate the collapse. Even though the fraction of primordial binaries in GCs is believed to be only a few per cent (e.g. Hurley et al. 2007; Davis et al. 2008), the binding energy of a single hard binary is sufficient to significantly slow down or perhaps even prevent core collapse (Hut et al. 1992; Heggie et al. 2006). On the other hand, because the relaxation time is inversely proportional to the mean stellar mass, the acceleration of core collapse due to mass segragation is roughly proportional to the increase in the mean mass, which in the core of M 15 is about a factor $1.19/0.43 \sim 3$ (Dull et al. 1997).

The detailed inclusion of these competing mechanism is beyond the scope of this paper, but to investigate the effect of a changing collapse rate on the encounter rate, we assume a 50% faster core collapse (and expansion) than the fiducial M 15 core evolution model. At the same time, this implies a lower initial concentration of $c_{\rm ini} \simeq 1.47$. The results of this "faster collapse" model on the encounter rate are shown with dashed curves in Figures 13–16, and 19. As can be seen from Figure 16, the main effect is a lowering of the global encounter rate by about 24% with respect to the fiducial model to $R_{\rm enc} \simeq 41\,{\rm yr}^{-1}\,{\rm Gpc}^{-3}$ at the peak, which remains around $z \sim 0.7$.

We already mentioned in Section 4.2 that after deepest core collapse the core can undergo fluctuations, either due to gravothermal oscillations (Bettwieser & Sugimoto 1984; Goodman 1987), or as a result of the stochastic nature of binary burning (Giersz & Heggie 2009). In either case, these fluctuations can result in change in the core radius $r_{\rm c}$ by factors of a few, and even order of magnitude changes in the core density $\rho_{\rm c}$. We do not attempt to capture this fluctuating nature, but we consider here a possible consequence of it. Because the (central) relaxation time is inversely proportional to $\rho_{\rm c}$, only a relatively small fraction of the time during an oscillation

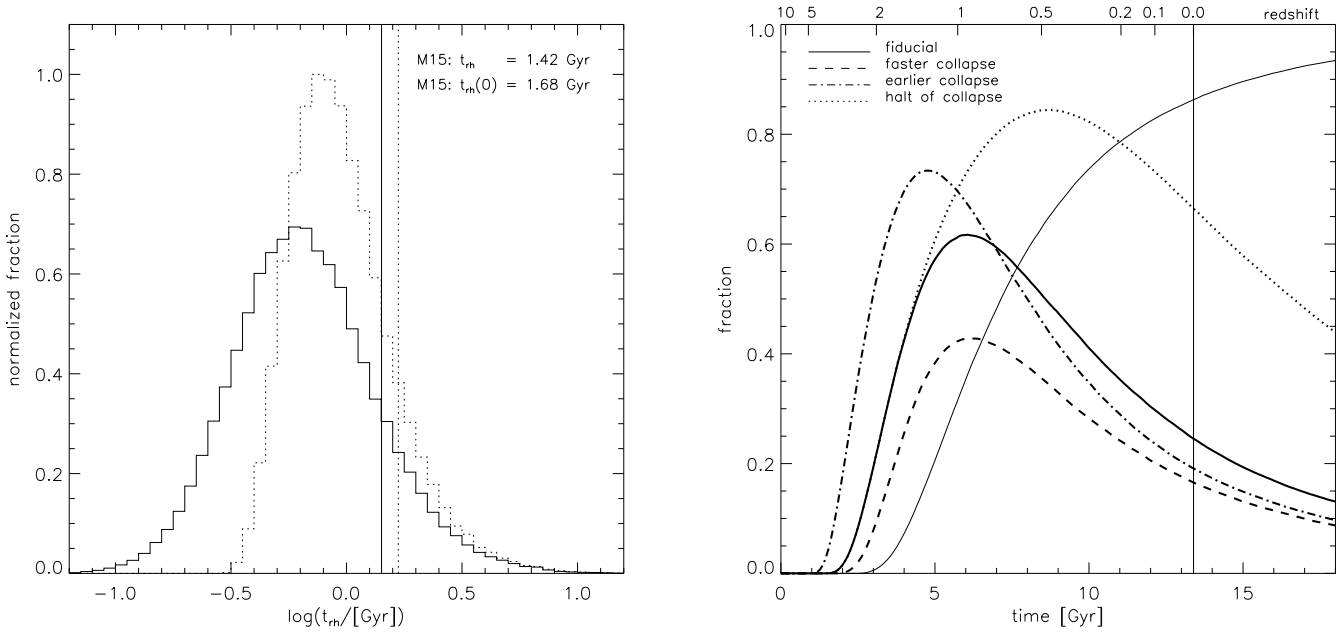

FIG. 14.— The *left panel* shows the distribution of half-mass relaxation times $t_{\rm rh} \propto r_h^{3/2} M^{1/2}$, based on the independent distributions in half-mass radii r_h and total mass M of globular clusters. This results in the solid histogram, which turns into the dotted histogram for initial half-mass relaxation times $t_{\rm rh}(0)$. The vertical lines show that M 15 has a larger than average half-mass relaxation time, so we expect that currently more than half of all GCs are already past reaching deepest core collapse. This is confirmed by the thin solid curve in the *right panel*, showing the fraction of GCs that past reaching deepest core collapse as function of time. However, in this fiducial core evolution model it is likely that some time after deepest core collapse the GCs are not anymore *observed* to be post-core-collapse because the core is expanding. Henceforth, to estimate the fraction of observed post-core-collapse GCs, we only count at a given time GCs that are in the late collapse or early expansion phase when the core is smaller. The resulting thick curves show that for the first three models the current fraction (vertical solid line) is similar to the fraction of $\simeq 20\,\%$ of post-core-collapse GCs observed in the Milky Way. Only the fourth halt-of-collapse model predicts a much higher fraction because the core properties are held fixed after deepest collapse.

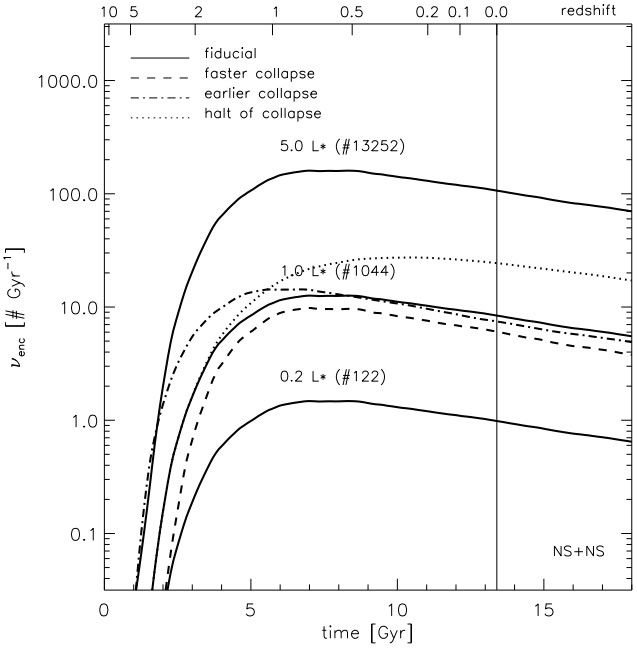

FIG. 15.— An *average* encounter rate between two neutron stars in the core of globular clusters per host galaxy with luminosity $L_{\rm gal} = \{0.2, 1.0, 5.0\} \times L\star$. The expected number of GCs per host galaxy, given in brackets, follows from McLaughlin (1999). For each globular cluster, the collision rate of M 15 is re-scaled by the half-mass relaxation time $t_{\rm rh} \propto r_h^{3/2} M^{1/2}$, randomly drawn from the independent distributions in half-mass radii r_h and total mass M of globular clusters. The meaning of different line styles is the same as in Fig.13.

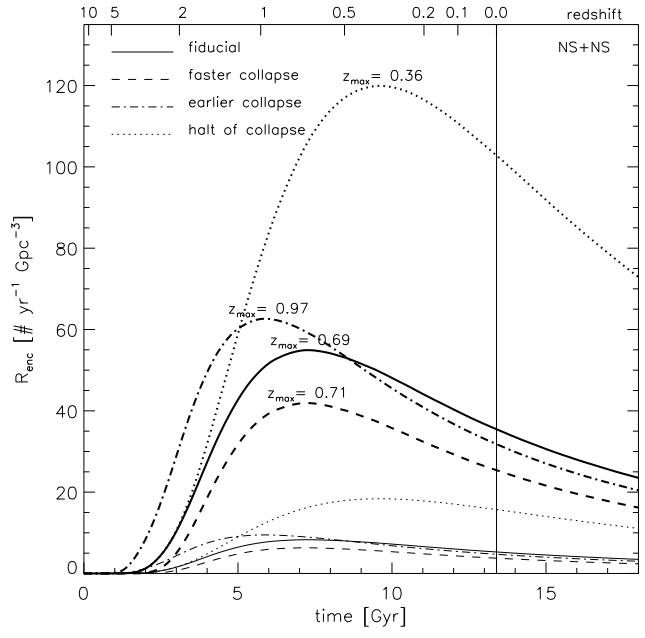

FIG. 16.— The predicted *global* rate of close encounters between two neutron stars in the cores of globular clusters, per volume of space and as function of time (or redshift at the top). The values are computed from combining the average collision rate per host galaxy (Fig. 15) with the galaxy luminosity density distribution. The meaning of different line styles is the same as in Fig.13.

will be spent at large ρ_c and correspondingly small r_c. Still, if we happen to observe a post-collapse GC during this special time at the "peak" of the fluctuation, we will underestimate the time elapsed since deepest collapse under our assumption of a steady expansion in our fiducial core evolution model. To investigate the possible effect on the encounter rate, we consider a shift the time of deep core collapse back in time by an amount of 2.6 Gyr, i.e., half of the duration of the late-phase collapse. As a consequence, the early-phase collapse is shorter by the same amount and the initial concentration increases to $c_{\rm ini} \simeq 1.79$. The smooth expansion model in this case predicts a current core radius and core density that are respectively almost 65% larger and a factor 3 smaller than the observed values of $r_c = 0.05\,{\rm pc}$ (Noyola & Gebhardt 2006) and $\rho_c = 6.5 \times 10^6\,{\rm M}_\odot\,{\rm pc}^{-3}$ (van den Bosch et al. 2006). The results of this "earlier collapse" model on the encounter rate are indicated by the dash-dotted curves in Figures 13–16, and 19. Figure 16 shows that the global encounter rate is increased by about 14% with respect to the fiducial model to $R_{\rm enc} \simeq 62\,{\rm yr}^{-1}\,{\rm Gpc}^{-3}$ at the peak, which occurs earlier, at $z \sim 1.0$. The latter is directly related to the applied shift in time, whereas the former is the result of more GCs reaching deep collapse in $t_{\rm age} = 13\,{\rm Gyr}$ (see also Figure 14).

The above faster and earlier collapse models imply respectively a lower and higher initial concentration for M 15 than used in the fiducial model. For each model, we then fixed the initial concentration of all GCs to that of M 15 when computing the average encounter rate. It is already very difficult to infer the initial concentration for M 15, let alone the distribution of initial concentrations for the population of old GCs. Even so, we have recomputed the average encounter rate adopting a Gaussian distribution in $c_{\rm ini}$, with a mean at the initial concentration of M 15 and with dispersion in the range $[0, 0.3]$. As a result of the dispersion, the rate of dissolution $\xi_{\rm dis}$ is not anymore fixed to that of M 15, which in turn leads to an additional broadening in the half-mass relaxation distribution when converting from current $t_{\rm rh}$ to initial $t_{\rm rh}(0)$ values. However, since the resulting variations in the conversion are typically less than $\sim 0.1\,{\rm Gyr}$, the effect on the average encounter rate is very small. Changing the mean, as we do in the faster and earlier collapse models, does have a significant effect on the average encounter rate. Nevertheless, we see from Figure 16 that the evolution of the global encounter rate is quite similar even for significant deviations from the fiducial mdoel. In other words, as long as M 15 is indeed representative of an (old) GC that underwent core collapse and expansion, we expect our predictions for the encounter rates to be robust.

4.5. *Binaries*

We have not included the potentially important effect of binaries in our encounter rate calculations. The fraction of primordial binaries in GCs is thought to be only a few per cent (Hurley et al. 2007), as confirmed by measuring photometric binaries beyond the half-light radius (see e.g. Davis et al. 2008). In the core of GCs tidal captures can significantly increase the fraction of binaries. Placing useful observational constraints on the fraction of binaries in the core is not an easy task because many of them could be dark as a result of binary-single interactions in which the more numerous main sequence stars (MS) and white dwarfs (WD) are replaced by compact remnants. Binary systems have a larger cross section for intersection and they mass segregate faster into the denser core than individual stellar objects. Three-body interactions are thus indeed likely to create compact binaries in the cores of GCs, including double neutron star (NS-NS) and black hole–neutron star (BH-NS) systems. As already noted in the Introduction, the merger of such dynamically formed compact binaries is potentially an important channel for the production of SGRB progenitor systems (Grindlay et al. 2006), different from the close encounters between single compact stellar objects we have considered so far. As we discuss below in 4.5.2, for encounters involving the exchange of a main sequence star with a neutron star or a black hole, the resulting separation will be too large for coalescence to take place in less than a Hubble time. Thus this channel is unlikely to contribute to the overall formation rate of viable SGRB progenitors. The occurrence of a direct impact may release a substantial amount of energy, but whether this can lead to the conditions required for SGRB production remains to be evaluated.

The three main ways to arrive at compact binaries are (i) primordial compact binaries, (ii) primoridal binaries of which the non-compact member(s) are replaced by compact objects via one (or two) exchange interactions, and (iii) the same as (ii) but starting from binaries which themselves are first formed through tidal capture of two single stellar objects. We consider all three ways below and show that in the cores of GCs, the latter dominates the formation rate of compact binaries, but is not, as commonly believed, dominant over the rate of close encounters between two single compact objects. While SGRBs are potentially created instanteneously when two compact objects closely encounter each other, the separation of the compact binary has to be small enough such that the time for the compact objects to merge, in addition to the formation time, is less than the Hubble time.

Note that we expect very little contribution to the close encounter rate from interactions between a single compact object (NS or BH) and a compact object that is a member of a binary which also contains a extended object (MS or WD). Even though we show below that the fraction of the latter binaries can be(come) significant, in nearly all cases the (exchange) interaction will be with the extended object (e.g. Sigurdsson & Phinney 1993).

4.5.1. *Primordial compact binaries*

The formation of primordial binaries follows the cosmic star formation rate which peaks at high redshift $z \sim 3$ (e.g. Hopkins & Beacom 2006). Primordial binaries with two massive stars ($\gtrsim 8\,{\rm M}_\odot$) that survive the mass loss and possible asymmetry of the supernova explosion of the secondary provide compact NS-NS and BH-NS binaries. They potentially could produce SGRBs at high redshift with a distribution extending to lower redshift depending on the range of initial binary separations and thus merger times. However, even if a non-neglible fraction of primordial massive binaries survive and result in close compact binaries ($\sim 10^{-2.5}$, Narayan et al. 1991), massive binaries are only a very small fraction of all primordial binaries for a reasonable, not too top-heavy initial mass

function ($\sim 10^{-4.5}$, for an IMF with a Salpeter power law slope from $100\,M_\odot$ down to $0.3\,M_\odot$, and constant down to $0.1\,M_\odot$). In GCs with already at most a few per cent primordial binaries ($\sim 10^{-1.5}$, Hurley et al. 2007; Davis et al. 2008) and likely additional complications to form and retain compact binaries (see also Ivanova et al. 2008), their possible contribution to producing SGRBs should be negligible; the GCs in the Milky Way contain a total of $\sim 10^{7.5}$ stars, which implies that we expect only ~ 1 primordial compact binary formed in the GCs of the Milky Way.

However, in the "field" of a galaxy the primordial binary fraction is of order unity and the vast amount of them results in a number of compact binaries that is not anymore insignificant; we expect $\sim 10^5$ primordial compact binaries formed in the "field" of the Milky Way (see, e.g. Narayan et al. 1991; Phinney 1991, for initial estimates). Merger rate calculations for such primordial binaries in the galactic field have become increasingly sophisticated (Kalogera et al. 2004; O'Shaughnessy et al. 2005, 2008, 2010), and now consider not only various stellar evolutionary channels, but also different host galaxy types (spiral vs. elliptical). The results are still hindered by the fact that there is a small number of observed systems, giving broad estimates in the range 1–$100\,\mathrm{yr}^{-1}\,\mathrm{Gpc}^{-3}$.

4.5.2. *Dynamically formed compact binaries*

Compact binaries formed dynamically in GCs have long delay times between compact object birth and binary formation as they have to wait for collapse of the core (Hopman et al. 2006). This helps their formation in three ways: (i) mass segregation increases the relative fraction of heavier-than-average binaries as well as compact remnants in the core, (ii) tidal capture increases the binary fraction in the core, in particular the "hard" binaries with small separations (whereas the "soft" binaries with large separations are being "ionized"), (iii) the high core density allows three-body exchange interactions in which a member of an existing binary is replaced with a compact remnant. Henceforth, we expect in the cores of GCs the compact binary formation rate to follow the close encounter rate, with a similar peak around $z \simeq 0.7$ as shown in Figure 16. Whereas after this initial delay the potential production of SGRBs is nearly instantaneous in the proposed encounter scenario, there is an additional delay in the binary merger scenario given by the rate of angular momentum losses through gravitational waves.

For a NS-NS binary dynamically formed around $z \simeq 0.7$ to merge within the next $\simeq 6$ Gyr through the emission of gravitational waves, the binary separation required is $a \lesssim 3.93\,R_\odot$. As mentioned above, most of the compact binaries in GCs are expected to be formed through three-body exchange interactions: a NS (average mass $1.4\,M_\odot$, and average radius 10 km) replaces the less-massive main-sequence star (MS; $0.4\,M_\odot$, 3.3×10^5 km) or white dwarf (WD; $0.5\,M_\odot$, 1.1×10^4 km) member in an existing binary with a NS. The latter NS-MS or NS-WD binary might be itself the result of a previous similar three-body exchange interaction with a MS-MS, WD-MS or WD-WD binary. We assume as minimum separation of these binaries the closest distance before ignition of mass transfer occurs (Paczyński 1971). This yields $a \gtrsim 1.72\,R_\odot$ and $a \gtrsim 0.054\,R_\odot$ for NS-MS and NS-WD binaries, respectively. We obtain similar lower limits of about 1.312, 1.365, and 0.043 in units of $R_\odot$ for MS-MS, WD-MS, and WD-WD binaries, respectively.

Even though after each exchange the binary hardens, the binary separation after an exchange, $a_{\rm fin}$, is typically larger than the binary separation before the exchange, $a_{\rm ini}$. Sigurdsson & Phinney (1993) show that the distribution of $a_{\rm fin}/a_{\rm ini}$ strongly peaks around the mass ratio m_f/m_e, between the single stellar object from the "field" and the stellar object "exchanged" from the binary, but with a long tail towards lower values. Taking for $a_{\rm ini}$ the minimum separation of each binary, we compute the median of the latter distribution[3] to arrive at the average $a_{\rm fin}$ after the first exchange interaction, and repeat this for the MS-MS, WD-MS, and WD-WD binaries that require a second exchange interaction to arrive at a NS-NS binary. For all three binaries with a MS as a member the resulting *minimum* binary separations (5.21, 12.8 and 12.4 in units of $R_\odot$ for NS-MS, MS-MS, and WD-MS, respectively) are larger than the above *maximum* binary separation for merger of the dynamically formed NS-NS binary ($3.93\,R_\odot$ for merging within $\simeq 6$ Gyr). Note that this is still the case even when we ignore the time to reach core collapse and allow the merger to take a full Hubble time, corresponding to a maximum binary separation of $4.8\,R_\odot$. On the other hand, a NS-WD binary results in a NS-NS binary with a minimum separation $a \gtrsim 0.126\,R_\odot$ well below the maximum for merging. Similarly, a WD-WD binary yields a NS-WD binary with $a \gtrsim 0.102\,R_\odot$ after the first exchange, and a NS-NS binary with $a \gtrsim 0.240\,R_\odot$ after the second exchange.

We assume that the formation rate of these binaries through three-body exchange interactions follows that of the collision rate, but with a different amplitude, which we estimate below.

4.5.3. *Compact binaries from primordial binaries*

Here we estimate the rates at which compact binaries in the cores of GCs are dynamically formed from primordial binaries, of which one or both members are non-compact stellar objects. We take $f_{\rm pri} = 0.02$ for the total fraction of primordial binaries in GCs, which is not well known but thought to be at most a few per cent (e.g. Hurley et al. 2007; Davis et al. 2008). To derive the fraction of primordial binaries that have a NS and a WD, we adopt an IMF with Salpeter power-law slope from $100\,M_\odot$ down to $0.3\,M_\odot$, and constant down to $0.1\,M_\odot$. Supposing that stars above $20\,M_\odot$ evolve into black holes (BHs), stars above $7\,M_\odot$ turn into SNe, stars above $0.8\,M_\odot$ end their life as WDs, and lower-mass stars are still in the MS, we find corresponding number fractions of about 0.0012 0.0043 0.1014, and 0.8930 for BH, NS, WD, and MS stars, respectively. While we start with drawing the masses of the primary and secondary, M_1 and M_2, indepdently from the IMF, we also consider the case that the mass ratio M_2/M_1 is distributed uniformly in the range from zero to unity. The former case is fully consistent with observed (spectroscopic) bi-

[3] We adopt an approaching velocity from infinity of $v_\infty = 2\sigma_{\rm c} \simeq 20\,\mathrm{km\,s}^{-1}$, but the results are not sensitive to the precise value that is adopted.

naries with longer periods ($P > 10^3$ days), but there are indications of a flatter distribution in mass ratios for the shorter-period binaries, possibly because stars that form close to each other become closer in mass by reaching an equilibrium in mass transfer. We adopt a lognormal distribution in binary periods P (in days) with mean $\mu_{\log P} = 4.8$ and standard deviation $\sigma_{\log P} = 2.3$ (Duquennoy & Mayor 1991).

We first consider the formation of NS-NS binaries from primoridal NS-WD binaries through a single exchange interaction. With the masses of the primary and secondary independently drawn from the IMF, we expect a fraction $f_{\rm NS-WD,pri} \simeq 8.81 \times 10^{-4}$ of all primordial binaries to be a NS-WD binary. Together with the stars and compact remnants that are heavier than the MS stars, the binary sinks to the core of a GC. During deep core collapse the NS-WD undergoes a three-body exchange interaction with a NS for which we adopt the number fraction $f_{\rm NS} \simeq 0.547$ of M 15 (Dull et al. 1997). We only count the NS-WD binaries with separations in the range $[0.054, 1.669]\,{\rm R}_\odot$. The lower limit is set to avoid stable mass transfer, while the upper limit increases after the exchange interaction to the maximum separation of $3.93\,{\rm R}_\odot$ allowed for merger of the dynamically formed NS-NS binary within $\simeq 6$ Gyr. Given the above lognormal distribution in binary periods, the fraction of NS-WD binaries in this range of separations is $f_{\rm sep} \simeq 1.83 \times 10^{-2}$. The corresponding mean separation is $\overline{a} \simeq 0.829\,{\rm R}_\odot$. We now obtain the rate from eq. (6) with $R_{\rm min} = \overline{a} + r_{\rm NS} \simeq 0.829\,{\rm R}_\odot$, $f_1 = f_{\rm pri}\, f_{\rm NS-WD,pri}\, f_{\rm sep} \simeq 3.23 \times 10^{-7}$, $f_2 = f_{\rm NS} \simeq 0.547$, and $m_1 + m_2 \simeq 2 \times 1.4 + 0.5 = 3.3\,{\rm M}_\odot$. In this way, we predict that the rate $R_{\rm dyn}$ to turn a primordial NS-WD binary dynamically into a NS-NS binary that can merge within the next $\simeq 6$ Gyr, is a factor $R_{\rm dyn}/R_{\rm col} \simeq 4.02 \times 10^{-2}$ smaller than the collision rate, and a factor $R_{\rm dyn}/R_{\rm tid} \simeq 0.618 \times 10^{-2}$ smaller than the tidal capture rate.

We now turn to the additional dynamical formation of a NS-NS binary from a primoridial WD-WD binary through two subsequent three-body exchange interactions with a NS. We assume that the first exchange to form the NS-WD binary happens some time before deepest core collapse, with a formation rate that can be computed in the same way as above. The fraction of primodial binaries that are WD-WD binaries is about $f_{\rm WD-WD,pri} \simeq 1.03 \times 10^{-2}$. We count the WD-WD binaries with separations in the range $[0.043, 0.708]\,{\rm R}_\odot$, with the lower limit again to avoid stable mass transfer, while the upper limit increases after two subsequent exchange interactions to the maximum separation of $3.93\,{\rm R}_\odot$ allowed for merger of the dynamically formed NS-NS binary within $\simeq 6$ Gyr. This range in separation corresponds to a fraction $f_{\rm sep} \simeq 1.10 \times 10^{-2}$ and mean separation $\overline{a} \simeq 0.371\,{\rm R}_\odot$. We then use as before eq. (6) with $R_{\rm min} \simeq 0.371\,{\rm R}_\odot$, while we set $f_1 = f_{\rm pri}\, f_{\rm NS-WD}\, f_{\rm sep} \simeq 2.27 \times 10^{-6}$, and $m_1 + m_2 \simeq 1.4 + 2 \times 0.5 = 2.4\,{\rm M}_\odot$. As in Section 4.2, we assume $f_2 = f_{\rm NS}(t)$ to vary from its primordial value to 0.547 during the early-phase collapse, and then to remain the same during the late-phase collapse. We intergrate the resulting rate of exchange interactions between a primordial WD-WD binary and single NS over the full duration of the core collapse phase. This yields the expected number ($\simeq 4.24 \times 10^{-4}$) of dynamically formed NS-WD binaries with separations within the above range. We then divide this number by the number of stellar systems ($\simeq 2.86 \times 10^3$) in the core $N_c = (4\pi/3) n_c r_c^3$ at deepest core collapse to arrive at a fraction $f_{\rm NS-WD,dyn} \simeq 1.48 \times 10^{-7}$. Next, we repeat the rate computation but now for dynamically forming a NS-NS binary in a second exchange interaction with $f_1 = f_{\rm NS-WD,dyn}$, $f_2 = f_{\rm NS} \simeq 0.547$, $m_1 + m_2 \simeq 2.4\,{\rm M}_\odot$, and $R_{\rm min} = 0.873\,{\rm R}_\odot$. The latter value arises from the above mean separation $\overline{a} \simeq 0.371\,{\rm R}_\odot$ after the first exchange interaction, multiplied by the (median) increase after the second exchange interaction. In this way, we find that the rate to dynamically form a NS-NS binary from a primordial WD-WD binary through two subsequent three-body exchange interactions is smaller than the collision rate by a factor $R_{\rm dyn}/R_{\rm col} \simeq 1.94 \times 10^{-2}$, and smaller than the tidal capture rate by a factor $R_{\rm dyn}/R_{\rm tid} \simeq 0.299 \times 10^{-2}$.

By combining the above two formation channels, we thus expect that the rate to dynamically turn primordial binaries into compact NS-NS binaries that can merge in time is smaller than the tidal capture rate by a factor $\simeq 0.916 \times 10^{-2}$. In case that the mass ratio M_2/M_1 of the primordial binary is uniformly distributed, the fraction of primordial NS-WD and WD-WD binaries increases to $f_{\rm NS-WD,pri} \simeq 4.76 \times 10^{-3}$ and $f_{\rm WD-WD,pri} \simeq 7.18 \times 10^{-2}$, i.e., a factor $\simeq 5.41$ and $\simeq 6.98$ higher than when M_1 and M_2 are independently drawn. As a result, the rate to form compact NS-NS binaries increases by a factor $\simeq 5.92$, but is still only a fraction $\simeq 5.43 \times 10^{-2}$ of the tidal capture rate.

A similar calculation for compact BH-NS binaries dynamically formed from primordial binaries shows that also in this case the minimum separations of primordial binaries with a MS star as a member are larger than the maximum separation of $\lesssim 6.34\,{\rm R}_\odot$ for which the BH-NS can merge within $\simeq 6$ Gyr. However, BH-NS binaries can form dynamically from primordial NS-WD or BH-WD binaries via a single exchange interaction with respectively a BH or NS, or from primoridal WD-WD binaries via two subsequent exchanges interaction with both a NS and a BH. We compute the rate for each of these formation channels in the same way as above. We assume that the fraction of BHs relative to the (changing) fraction of NSs remains equal to the primoridal fraction, i.e., $f_{\rm BH}/f_{\rm NS} \simeq 0.283$ throughout. If instead of chosing the masses of the primary M_1 and secondary M_2 of the primordial binary indepedently, we assume that the mass ratio M_2/M_1 is uniformly distributed, the fraction of primordial NS-WD, BH-WD and WD-WD binaries increases by a factor 5.41, 1.73, and 6.98, respectively. At the end, the combination of the three formation channels yields a formation rate of compact BH-NS binaries is smaller than the tidal capture rate between a single BH and NS by a factor $\simeq 0.593 \times 10^{-2}$ if M_1 and M_2 are independently drawn, and a factor $\simeq 1.88 \times 10^{-2}$ when M_2/M_1 is uniformly distributed.

4.5.4. *Compact binaries from tidally captured binaries*

It is clear from the above calculations that in the cores of GCs close encounters between single compact objects are significantly more likely than mergers of compact bi-

naries that are dynamically formed from primordial binaries. When starting instead from binaries that are formed through tidal captures the chance of dynamically forming and merging a compact binary can be much higher as we show below. As before binaries with a MS as a member are omitted, because they result after exchange interaction(s) in compact binaries with minimum separations that are larger than the maximum separation allowed for them to merge in time.

We first consider the formation of NS-NS binaries from tidally captured NS-WD binaries. To compute the fraction of tidally captured NS-WD binaries, we integrate the tidal capture rate between a NS and WD over time until deepest core collapse, and then divide by the number of stellar systems in the core. The tidal capture rate is given by eq. (6) after substitution of $R_{\rm min}$ from eq. (8). We assume $f_1 = f_{\rm NS}(t)$ and $f_2 = f_{\rm WD}(t)$ to vary during the early-phase collapse from their primordial values to respectively 0.547 and 0.218, and then to remain the same during the late-phase collapse. This yields the expected number ($\simeq 8.86$) of tidally captured NS-WD binaries with (pericenter) seperations up to $0.109\,{\rm R}_\odot$. This is well below the upper limit of $1.669\,{\rm R}_\odot$ that increases after the exchange interaction to the maximum separation of $3.93\,{\rm R}_\odot$ allowed for merger of the dynamically formed NS-NS binary within $\simeq 6\,$Gyr. The lower limit to avoid stable mass transfer is $0.054\,{\rm R}_\odot$, and gives rise to a fraction $f_{\rm sep} \simeq 0.511$ of tidally captured NS-WD binaries with separations in this allowed range, and with corresponding mean separation of $\overline{a} \simeq 0.093\,{\rm R}_\odot$. Finally, we divide by the $\simeq 2.86\times10^3$ stellar systems in the core to arrive at a fraction $f_{\rm NS-WD,tid} \simeq 1.72\times10^{-3}$ of tidally captured NS-WD binaries. The calculation for the subsequent exchange reaction with a NS, is the same as above in Section 4.5.3 for the formation of NS-NS binaries from primordial NS-WD binaries, except that in eq. (6) we now have $f_1 = f_{\rm NS-WD,tid}$. In this way, we estimate that the rate $R_{\rm dyn}$ to turn a tidally captured NS-WD binary dynamically into a NS-NS binary that can merge within the next $\simeq 6\,$Gyr is a factor $R_{\rm dyn}/R_{\rm tid} \simeq 3.70$ larger than the tidal capture rate.

We now turn to the additional dynamical formation of a NS-NS binary from a tidally captured WD-WD binary through two subsequent three-body exchange interactions with a NS. Since the tidal capture rates between two WDs and between a WD and a NS are similar (Table 3), we expect the rate to be significantly less than just estimated for NS-NS binary formation from a tidally captured NS-WD binary, which only needs one subsequent exchange interaction. We assume that both the tidal capture of the two WDs and the first subsequent exchange happen before deepest core collapse. This means we first calculate the fraction of WD-WD binaries formed through tidal capture as function of time, i.e., $f_{\rm WD-WD,tid}(t)$. The calculation is the same as for $f_{\rm NS-WD,tid}$ above, but with $f_1 = f_2 = f_{\rm WD}(t)$, and we integrate the tidal capture rate up to time t, followed by division with the number of stellar systems in the core $N_c(t) = (4\pi/3)n_c(t)r_c(t)^3$ at that time. To have the WD-WD binary (pericenter) seperations up to $0.092\,{\rm R}_\odot$ within the allowed range of $[0.043, 0.708]\,{\rm R}_\odot$, implies $f_{\rm sep} \simeq 0.530$ and a mean separation of $\overline{a} \simeq 0.072\,{\rm R}_\odot$. Next, we substitute $R_{\rm min} = \overline{a} + r_{\rm NS} \simeq 0.072\,{\rm R}_\odot$, $f_1 = f_{\rm WD-WD,tid}(t)$, $f_2 = f_{\rm NS}(t)$ and $m_1{+}m_2 \simeq 2{\times}0.5{+}1.4 = 2.4\,{\rm M}_\odot$ in eq. (6). Integrating the resulting rate over the full duration of the core collapse phase, yields the expected number ($\simeq 4.08\times10^{-3}$) of dynamically formed NS-WD binaries from tidally captured WD-WD binaries. We then divide by the $\simeq 2.86\times10^3$ stellar systems in the core at deepest collapse, to arrive at a fraction $f_{\rm NS-WD,dyn} \simeq 1.43\times10^{-6}$. As above in Section 4.5.3, we repeat the rate calculation for dynamically forming a NS-NS binary in a second exchange interaction with a NS. In this way, we find that the rate to form a NS-NS binary dynamically from a tidally captured WD-WD binary through two subsequent three-body exchange interactions is smaller than the tidal capture rate by a factor $R_{\rm dyn}/R_{\rm tid} \simeq 0.555\times10^{-2}$.

By combining the above two formation channels, we thus expect that the rate to dynamically turn tidally captured binaries into compact NS-NS binaries that can merge in time is larger than the tidal capture rate by a factor $\simeq 3.71$. As expected, this factor is mainly the result of the first formation channel, of which the rate is much larger, by a factor $\simeq 667$, than the second formation channel. Next, we estimate in a similar way also the rates to dynamically form BH-NS binaries from tidally captured NS-WD or BH-WD binaries via a single exchange interaction with respectively a BH or NS, or from tidally captured WD-WD binaries via two subsequent exchanges interaction with both a NS and a BH. From the three formation channels together, we predict a formation rate of BH-NS binaries that is larger than the tidal capture rate between a single BH and NS by a factor $\simeq 8.42$. Again, the contribution from the third formation channel that involves two subsequent exchange interactions is much smaller, by factors $\simeq 72.8$ and $\simeq 371$, than the first and second formation channel.

4.5.5. *Merger versus encounter rate*

The above calculations provide an estimate of the relative frequencies of (binary) mergers and close encounters between two compact objects in the cores of GCs. Combining the results from Sections 4.5.1 – 4.5.4, we estimate for a compact NS-NS (BH-NS) binary a higher merger than tidal capture rate by a factor $\simeq 3.7$ ($\simeq 8.4$).

These estimates can be further improved by allowing a range in WD and MS star masses (instead of adopting mean masses of $0.5\,{\rm M}_\odot$ and $0.4\,{\rm M}_\odot$, respectively), by sampling the full distribution in the ratio of binary separations before and after a three-body exchange interaction (instead of taking the median value of $a_{\rm fin}/a_{\rm ini}$), and by including the formation and subsequent merger of compact binaries throughout the lifetime of a GC instead of concentrating on deepest core collapse with a peak around $z \simeq 0.7$). Also the binaries will interact among themselves, so that four-body interactions could become important, especially since the number of tidally captured binaries is increasing; when for all ten possible binary pairings from a BH, NS, WD and MS, we integrate the corresponding tidal capture rate up to the time of deepest collapse, we find a total of $\simeq 207$ dynamically formed binaries. Given the $\simeq 2.86\times10^3$ stellar systems in the core, we obtain a binary fraction of $\simeq 7.23\,\%$ compared to a primordial binary fraction of a few per cent. These and other improvements are clearly interesting but beyond the scope of this paper.

From the above estimates, we can conclude that in the

cores of GCs the rate of close encounters between two single compact objects can become similar to the rate of merging of two compact objects in a binary. The latter compact binaries most likely are formed through a three-body exchange interaction with a binary which itself originated from a tidal capture between a compact and non-compact (WD) stellar object (Section 4.5.4). The alternative dynamical formation of compact binaries from primordial binaries (Section 4.5.3) is less likely by about two orders of magnitudes. A main reason is that the fraction of primordial binaries in GCs is at most a few per cent, which in turn also implies that the number of primordial compact binaries in GCs is negligble, while they are thought to be the dominant source of SGRBs in the "field" of a galaxy (Section 4.5.1). While SGRBs are commonly assumed to orginated from compact binary mergers, we thus find that close encounters between two compact objects in the core of GCs can also provide a significant contribution.

5. DISCUSSION

Dense stellar systems in some ways are like an ecological network, where feedback is extremely important and apparently isolated events can have far-reaching consequences. In a globular cluster, as we discussed, dynamical interactions between passing stars can form new binaries and modify the properties and even the membership of existing binaries. Motivated by this, we have investigated the production of compact binaries via two and three body encounters. We find that event rates within globular clusters are expected to be significant, and can become similar to the overall production of merging compact binaries. This hints at the underlying possibility that SGRB progenitors may not be entirely restricted to the most widely favored scenario involving the merger of compact binaries in the field. Much of our effort in this section will therefore be dedicated to determining what are the expected characteristics of SGRBs arising from these encounters and how do they compare to recent observational constraints.

5.1. *Prospects for the production of SGRBs*

It is clear from the calculations presented in Section 2.4 that the formation of an accretion disk around the primary is a robust result, regardless of the initial orbital parameters (as long as disruption occurs, of course). The particulars of each case, however, are variable in several aspects, and can lead to interesting diversity.

First, and most importantly, the resulting disk mass is not always equal. This is crucial in terms of the available energy in the system, as it sets the overall scale for an accretion powered event that could produce a SGRB. We find that even for the relatively small variation in angular momentum (or equivalently, impact parameter) for black hole–neutron star encounters the resulting disk mass, $M_{\rm disk}$, varies almost by a factor of three. We have previously estimated (Lee, Ramirez-Ruiz & Granot 2005; Lee & Ramirez-Ruiz 2007) that the energy that can be potentially extracted from such disks to produce a GRB scales as $M_{\rm disk}^2$ for neutrino powered events, and as $M_{\rm disk}$ for magnetically dominated bursts. The range in mass thus possibly spans an order of magnitude when converted to total energy release.

Second, the nature of the primary itself can produce a different outcome. The "cleanest" scenario involving a black hole leads to accretion in the hypercritical regime discussed above. However, for double neutron star collisions, a range of possibilities remains. For the one calculation of this type we have performed, at the end of the simulation the central core is rapidly rotating and is surrounded by a massive envelope. If the core can avoid collapse, it is possible that the rapid rotation will wind up the magnetic field to large magnetar-like values (Price & Rosswog 2006) and allow for repeated episodes of energy release (Usov 1992; Kluźniak & Ruderman 1998).

Third, the presence of large tidal tails in which material will fall back onto the central object at a later time is a generic feature of the present set of calculations. The mass involved in these structures is considerably larger than for binary mergers for the reasons already mentioned in Section 2.5. As the impact parameter in the black hole neutron star collisions increases, the mass in the tail can become even larger than that in the disk. Thus the properties of the fall back material will dominate the behavior at late times (Lee, Ramirez-Ruiz & Lopez-Camara 2009).

The differential energy distribution in the tails is shown in Figure 17. Material with negative energy is either in the torus surrounding the black hole, or in a portion of the tail that is bound to it. Fluid with positive energy will eventually leave the system. The thick black vertical line in each plot separates the torus and the tails morphologically, making it clear that a substantial portion of the tails is bound and will fall back. In the simple analytical estimates performed initially for stellar interactions with supermassive black holes, the distribution of mass with specific energy of the material from the disrupted star was constant, thus giving rise to a fall back accretion rate $\dot{M}_{\rm fb} \propto t^{-5/3}$, computed assuming ballistic trajectories (Rees 1988). We have computed the corresponding accretion rate here as well, also by assuming that the fluid in the tails is on ballistic trajectories in the potential well of the central mass (allowing us to follow it for a much longer time). The more complex interaction we have outlined for the case of comparable masses produces a different decay law, closer to $\dot{M}_{\rm fb} \propto t^{-4/3}$, see Figure 18. There is also variability on shorter time scales superposed on this decay, due to inhomogeneities in the tidal tails. Characterizing this requires a full hydrodynamical and thermodynamical treatment of the motion in the tails at late times (Rosswog 2007; Lee, Ramirez-Ruiz & Lopez-Camara 2009; Metzger et al. 2009).

Essentially, the bulk of the material in the tail will return to the vicinity of the compact object within a few seconds. As it has finite angular momentum, it will not directly impact the primary but describe an accentric orbit around it. Moreover, since it is not composed of test particles but is a fluid stream, dissipation close to periastron will circularize the orbit at a radius roughly equal to the distance from which it was ejected in the first place. If angular momentum transport processes are present and the gas is able to cool with some efficiency, it will then form an accretion disk and feed the primary with mass and energy. The viscous time scale will be

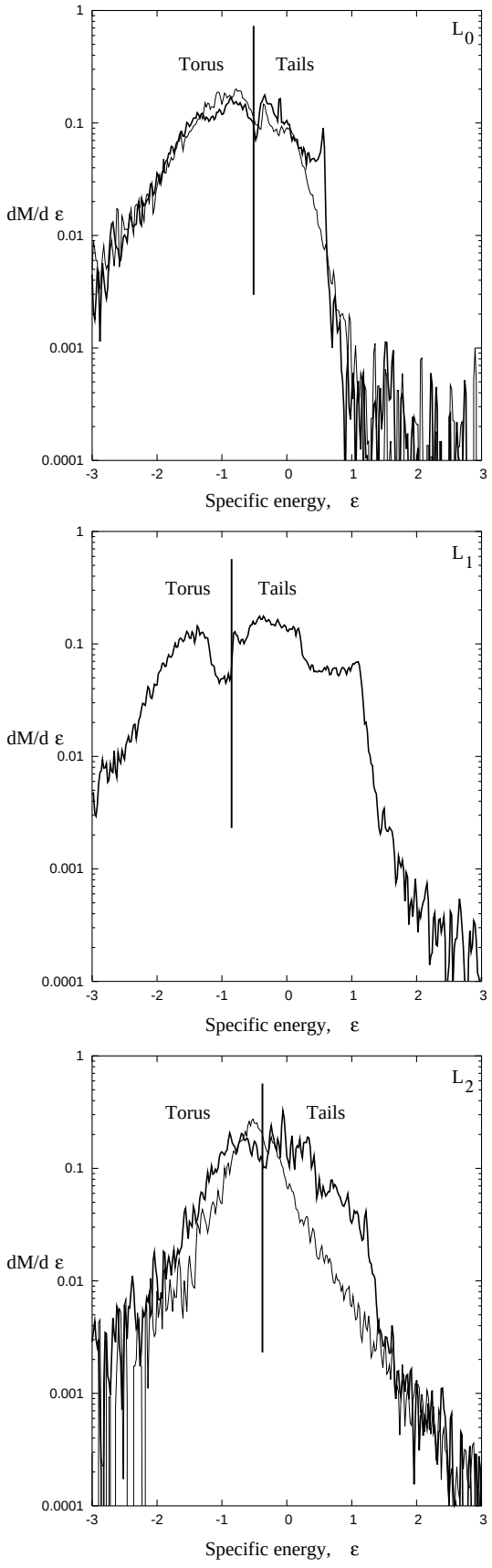

FIG. 17.— Differential distribution of mass with specific energy for the fluid at the end of runs L_0, $L_0\Gamma_{5/3}$, L_1, L_2 and $L_2\Gamma_{5/3}$. The thick (thin) lines are for $\Gamma = 2$ ($\Gamma = 5/3$). The vertical line marks the morphological division between matter that lies in the torus around the black hole and that contained in the tidal tails. A fraction of the latter has positive energy and will escape the system.

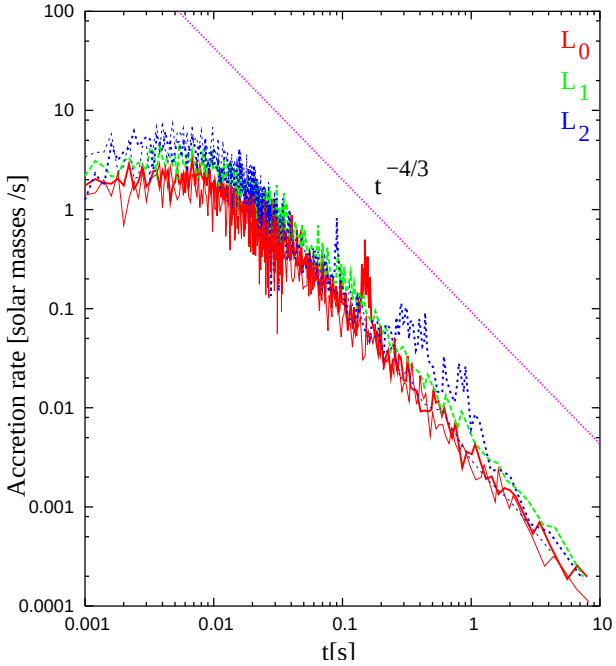

FIG. 18.— The fall back accretion rate onto the central object from tidal tails (in solar masses per second) is shown for runs L_0, $L_0\Gamma_{5/3}$, L_1, L_2 and $L_2\Gamma_{5/3}$, along with a reference power law with decay index $-4/3$. The thick (thin) lines are for $\Gamma = 2$ ($\Gamma = 5/3$).

much longer than the dynamical re-injection time scale, and thus for transport purposes it will be as if a disk had been formed practically impulsively around the black hole (or neutron star), subsequently evolving on a secular time scale. It is thus possible, in principle, to account generically in this scenario for a prompt episode of energy release as well as for activity many dynamical time scales later.

Finally, we have shown also that the nature of the secondary (neutron star vs. white dwarf) will lead to a substantially different final configuration. In the white dwarf case the accretion disk is much larger, and thus the densities are substantially lower (the total mass being comparable). The key question in this case is whether the gas can find an efficient mechanism to cool, and thus accrete. Otherwise the material will only be blown to large radii and not release enough gravitational binding energy to account for the energy budget of a GRB.

5.2. *Time delay*

The observed event rate of SGRBs as function of redshift can provide constraints on a time delay between the formation of the progenitors and the explosion (Guetta & Piran 2005, 2006; Nakar et al. 2006; Bloom & Prochaska 2006). SGRBs exhibit great diversity in terms of their host galaxies, and a cursory comparison of the redshift distribution of SGRBs with the universal star formation rate (SFR) reveals what appears to be a significant time delay of a few Gyr. A large progenitor lifetime would help explain the apparent high incidence of galaxy cluster membership (Pedersen et al. 2005; Bloom et al. 2006; Berger 2007), while on the other hand, shorter lifetimes are required to explain the population of SGRBs at moderately high redshift (Berger et al. 2007; Graham et al.

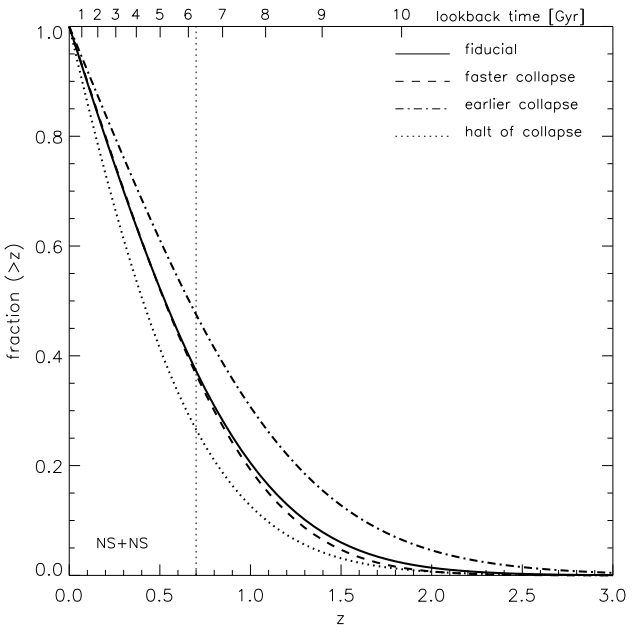

FIG. 19.— The predicted cumulative redshift distribution of SGRBs under the assumption that they are produced by tidal capture of two neutron stars in the cores of globular clusters. The meaning of different line styles is the same as in Fig.13.

2009). Short delays have been pointed out as a possibility for merging binaries directly from populations synthesis calculations (Belczynski, Bulik & Kalogera 2002; Belczynski et al. 2006; O'Shaughnessy et al. 2008), and could be responsible for a significant fraction of the observed event rate.

An alternative approach for constraining the distribution of time delays may be to use the event rates of SGRBs in different types of galaxies (Gal-Yam et al. 2008; Zheng & Ramirez-Ruiz 2007). On average, early-type galaxies have their stars formed earlier than late-type galaxies, and this difference, together with the time delay between progenitor formation and SGRB outburst, inevitably leads to different burst rates in the two types of galaxies. For instance, the morphological types for SGRBs reflect a higher incidence of early-type galaxies than Type Ia supernovae and this would suggest associated progenitor lifetimes significantly exceeding a few Gyrs (Zheng & Ramirez-Ruiz 2007). Making more quantitative statements about the ages of the progenitor systems is not only hampered by small number statistics but also from the lack of robust predictions of the distribution of merger sites as a function of time.

Observational evidence for a significant time delay between tracers of star formation and SGRB outburst excludes that the production of SGRBs is exclusively related to the short time-scale for evolution and death of massive stars, which are believed to be the progenitors for long GRBs. However, significant time lags between the cosmic star formation rate and the SGRB redshift distribution occur naturally if the progenitor is a compact binary in the field that merges (Cenko et al. 2008; Salvaterra et al. 2008; Hopman et al. 2006), as well as in the case of a close encounter between two compact stellar objects in a dense stellar environment. For a merger, the time delay reflects the time for the two compact objects to merge by emission of gravitational waves, while for close encounters a significant rate is only achieved when the stellar density rises significantly through the core collapse of a stellar cluster. Figure 19 shows our predicted cumulative redshift distribution for the progenitors of SGRBs assuming they are produced by tidal capture of two neutron stars in GCs. Further redshift determinations are required to help differentiate between various ways of forming a short GRB, although, as we argue next in Section 5.3, detailed observations of the astrophysics of individual GRB host galaxies may be essential before stringent constraints on the lifetime of short GRB progenitors can be placed.

5.3. *Galactic environment*

The observed offsets from what has been argued are the plausible hosts, if true, also holds important ramifications for the sort of viable progenitors (see Belczynski et al. 2006; Zemp, Ramirez-Ruiz & Diemand 2009). Very large offsets seen from early-type hosts would seem to be at odds with progenitor systems with small systematic kicks such as those occurring in globular clusters, although with such large physical offsets the possibility remains that the association with the putative host is coincidental. On the other hand, based on the small offsets from some low-mass galaxy hosts (Prochaska et al. 2006; Soderberg et al. 2006; Berger 2009; Bloom & Prochaska 2006), SGRB progenitors cannot all have large systematic kicks at birth and inherently large delay times from formation.

Compact binaries in the field are expected to experience a kick, leading to mergers away from their point of origin. The displacement depends on the distribution of kick velocities, merger times, and host masses, with predicted values in the range 10–100 kpc (Fryer et al. 1999; Belczynski et al. 2006; Zemp, Ramirez-Ruiz & Diemand 2009), depending on the formation channel, host galaxy type and mass. By contrast, GCs are expected to show on average moderate displacements: the spatial distribution of GCs peaks around the half-light radius —typically a few kpc— of the host galaxy. What is more, due to the large red giant star density in the GC core, there is the possibility for the interaction of the external shock with a denser external medium than that of the IGM (Parsons, Ramirez-Ruiz & Lee 2009).

If a significant fraction of SGRBs is indeed produced in GCs we also expect to see a strong preference for this scenario occurring in luminous host galaxies, because the number of GCs increases steeply with the host galaxy luminosity as $\propto L_V^{>1.5}$ (McLaughlin 1999), whereas the number of primordial binaries increases only as $\propto L_V$. Red, early-type galaxies are on average more luminous than blue, late-type galaxies, which would lead to a higher incidence of this kind of SGRB in ellipticals when compared to spiral galaxies. The current limited sample indicates that, if unidentified hosts are in fact ellipticals, SGRBs would be approximately evenly distributed between early and late-type hosts (Berger 2009). However, the morphology of galaxies changes with time due to internal (secular) evolution, and in particular when they merge. As a result, the fraction of late-type to early-type galaxies increases toward higher redshift, and hence SGRBs in GCs might occur also more frequently in spiral galaxies.

In other words, if (old) GCs are formed in the highest density peaks before reionization (e.g. Moore et al. 2006), and subsequently were accreted in galaxies through mergers, SGRBs or any other transient connected with GCs would provide a unique tracer of the hierchical build-up of galaxies. This look-back on galaxy evolution is of course limited by the observability of such transients, both due to their intrinsic brightness and the duration of the event, as well as due to the time delay discussed in Section 5.2. The latter time delay is probably also what limits the possible contribution from intermediate-age GCs which are thought to form in gas-rich galaxy mergers. The formation time of these intermediate-age GCs plus the time for their cores to collapse will significantly shift the potential production of SGRBs towards lower redshift with respect to old GCs.

Up to this point, we have argued for the production of SGRBs in GCs as oppposed to originating from primordial compact binaries within the host galaxy field, but we have not yet distinguised between mergers or close encounters between compact stellar objects in GCs. Like intermediate-age versus old GCs, we also expect the redshift distribution of SGRBs in the merger scenario to be skewed toward lower redshift than in the encounter scenario. From the global encounter rate in Figure 16, we expect a significant SGRB event rate only below $z \sim 1$. This is still consistent with SGRBs found recently around $z \sim 1$ (Berger et al. 2007), but is very challenging or perhaps impossible in case of the additional time delay in case of merging compact binaries.

5.4. *Nuclear clusters*

The high stellar densities in which both close encounters and three-body interactions become significant may, besides in the collapsed cores of GCs, also be reached in the nuclei of galaxies. Of particular interest are the nuclear (stellar) clusters (NCs) as they might also experience core collapse. NCs have been found in 50%–75% of both late-type and early-type galaxies, but they are absent in the elliptical galaxies brighter than absolute magnitude $M_B \sim -19$ (although this could in part be an observational bias due to the presence of steep central cusps), and the frequency of nucleation also falls to zero in dwarf galaxies fainter than $M_B \sim -12$ (see the review by Böker 2008). NCs have typical half-light radii ($\sim 3.5\,\mathrm{pc}$; Böker et al. 2002) similar to GCs, but their typical masses ($\sim 3 \times 10^6\,\mathrm{M}_\odot$; Walcher et al. 2005), and hence their average density is also higher than that of GCs by the same factor.

On the other hand, the half-mass relaxation time of NCs is about an order of magnitude longer than those in GCs, both due to their higher typical mass as well as due to the higher velocity dispersion of the surrounding galaxy. The latter results in a flow of energy from the galaxy to the NC, which opposes core collapse and might even lead to core expansion (Dokuchaev & Ozernoi 1985; Kandrup 1990). The result is a minimum compactness of NCs in order to resist expansion (Quinlan 1996; Merritt 2009), which is close to their observed sizes. This, together with their longer half-mass relaxation times when compared with GCs, argues against NCs experiencing core collapse and thus providing a fertile ground for the production of SGRBs via close encounters between compact stellar objects. In addition, the presence of a possible (super or intermediate) massive black halo in NCs (Seth et al. 2008) inhibts core collapse, and NCs with black holes always expand (Merritt 2009).

Still, it is possible that NCs were formed with a high initial concentration (and without an as yet significantly massive black hole) at the highest density peaks so that their cores collapsed early on. Later on the core and NC as a whole expanded, partly at least due to growing heat input from the surrounding galaxy of which the velocity dispersion increases as a result of its (secular and/or hierarchical) evolution. An additional and likely even stronger expansion of a NC is expected in case the host (dwarf) galaxy is stripped away when it is accreted by a larger galaxy; a formation history that is believed to be applicable also to the most massive GCs in the Milky (e.g Georgiev et al. 2009). In both cases, the currently observed larger size and longer half-mass relaxation time would not be an indication of a possible core collapse in the past.

If NCs indeed experienced such a core collapse significantly earlier than GCs, we expect from comparing the earlier collapse and fiducial model in Figure 16 that the SGRBs potentially produced through close encounters of compact objects in NCs will be skewed to higher redshift $z > 0.7$. At the same time, we expect the SGRB to be located in the center of typically a faint (nucleated) dwarf galaxy. Also, the multiple stellar populations observed in local nuclear clusters (e.g. Walcher et al. 2006) very likely imply on-going star formation at higher redshift. This is all in line with the recently observed high-redshift SGRBs and their host galaxy properties (Berger 2009), but clearly requires further study of NCs and in particular evidence for past core collapse.

We finally note that even though the presence of a central black hole inhibits core collapse and hence prevents short (two-body) relaxation times, secular resonant relaxation can operate on a much smaller time scale. This alternative relaxation process can increase the ellipticity of stellar objects on (near) Keplerian orbits, and hence not only bring them closer to the black hole (e.g. Rauch & Tremaine 1996), but also to each other. This increases again the change of close encounters, and, if it involves two compact objects, the potential to produce SGRBs in the vicinity of massive black holes.

6. SUMMARY AND CONCLUSIONS

It is evident from the work presented here that tidal capture in close encounters and collisions between compact stellar objects in the cores of GCs can provide a viable channel for the production of SGRBs at rates which are significant when compared to those from the mergers of primordial compact binaries, in both GCs and the field. For GCs with small primordial binary populations, we have argued that the formation of coalescing compact binaries which are capable of powering a SGRB is dominated by dynamical exchanges of NSs (BHs) with tidally formed WD-NS(BH) binaries and by the close encounters of NSs with NS/BHs.

Through a realistic though conservative calculation, we predict an event rate for the tidal capture and collision of two neutron stars in the collapsed core of a GC that steeply increases to $\sim 50\,\mathrm{yr}^{-1}\,\mathrm{Gpc}^{-3}$ around $z \sim 0.7$, and is followed by a gradual decline to $\sim 30\,\mathrm{yr}^{-1}\,\mathrm{Gpc}^{-3}$ at $z = 0$. This is consistent with the currently observed

event rate and redshift distribution of SGRBs. Furthermore, since the number of GCs both steeply increases with galaxy luminosity and peaks at the half-light radius of the host galaxy, we expect SGRBs to appear in both late and early-type galaxies and to be displaced from the galaxy center, in line with the cursory identification of and location in host galaxies.

Using detailed hydrodynamics simulations we have explored the collision of NSs with WD/NS/BHs for a range of system parameters, to complement previous knowledge on binary mergers. We have shown that close encounters involving neutron stars and/or black holes can account for both a prompt episode of energy release, as well as for activity many dynamical times later through a accretion disk formed from the re-infall of disrupted material expelled in a bound tail. Relatively small changes in the impact parameter of the close encounter, as well as the nature of the secondary clearly result in a significant diversity in the final configuration. The significant amount of material that is dynamically ejected comes from the multiple periastron passages experienced before full tidal disruption takes place, each one carrying a distinctive signature of its thermodynamical history. Thus, while it could contribute significantly to the observed abundance of r-process elements (Lattimer & Schramm 1974, 1976; Symbalisty & Schramm 1982; Freiburghaus et al. 1999), not all of it need do so in principle.

We thank J. Bloom, C. Fryer, J. Guillochon, D. Heggie, P. Hut, V. Kalogera, R. O'Shaughnessy, X. Prochaska, F. Rasio and S. Rosswog for useful discussions and comments on the draft. We thank both referees for constructive comments on this work, which helped improve the final version. Part of this work was carried out during visits to the Institute for Advanced Study in Princeton, the University of California in Santa Cruz, and the Instituto de Astronomía at UNAM, whose hospitatlity is gratefully acknowledged. This work was supported in part by CONACyT-83254 and DGAPA-UNAM-IN-113007 (WL), NASA NNX08AN88G and the David and Lucile Packard Foundation (ER), UCMEXUS (ER and WL) and NASA through Hubble Fellowship grant HST-HF-01202.01-A, awarded by the Space Telescope Science Institute, which is operated by the Association of Universities for Research in Astronomy, Inc., for NASA, under contract NAS 5-26555 (GvdV).

REFERENCES

Backer, D.C., Kulkarni, S.R., Heiles, C., Davis, M.M., Goss, W.M. 1982, Nature, 300, 615
Barthelmy, S. D. et al. 2005, Nature, 438, 994
Baumgardt, H., Heggie, D. C., Hut, P., & Makino, J. 2003, MNRAS, 341, 247
Baumgarte, T.W., Shapiro, S.L., Shibata, M. 2000, ApJ, 528 L28
Belczynski, K., Bulik, T., Kalogera, T. 2002, ApJ, 571, L147
Belczynski, K., Perna, R., Bulik, T., Kalogera, V., Ivanova, N., & Lamb, D. Q. 2006, ApJ, 648, 1110
Berger, E. 2007, ApJ, 670, 1254
Berger, E. 2009, ApJ, 690, 231
Berger, E. et al. 2005, Nature, 438, 988
Berger, E. et al. 2007, ApJ, 664, 1000
Bettwieser, E. & Sugimoto, D. 1984, MNRAS, 208, 493
Bloom, J. S. et al. 2006, ApJ, 638, 354
Bloom, J. S., Prochaska, J. X. 2006, AIP Conference Series, 836, 473
Böker, T. 2008, Journal of Physics Conference Series, 131, 012043
Böker, T., Laine, S., van der Marel, R. P., Sarzi, M., Rix, H.-W., Ho, L. C., & Shields, J. C. 2002, AJ, 123, 1389
Carter, B., Luminet, J.P. 1983, å, 121, 97
Cenko, S. B., Berger, E., Nakar, E., Kasliwal, M. M., Cucchiara, A., Kulkarni, S. R., Ofek, E., Fox, D. B., Harrison, F. A., Rau, A., Price, P. A., Gal-Yam, A., Dopita, M. A., & Penprase, B. E. 2008, ApJLetters submitted, arXiv:0802.0874v1
Chandrasekhar, S. 1961, *Hydrodynamic and hydromagnetic stability* (Oxford: Oxford University Press)
Chernoff, D. F. 1993, in ASP Conf. Ser. 50: Structure and Dynamics of Globular Clusters, ed. S. G. Djorgovski & G. Meylan, 245–+
Clark, G. W. 1975, ApJ, 199, L143
Cook, G.B., Shapiro, S.L., Teukolsky, S.A. 1994, ApJ, 424, 823
Davis, D. S., Richer, H. B., Anderson, J., Brewer, J., Hurley, J., Kalirai, J. S., Rich, R. M., & Stetson, P. B. 2008, AJ, 135, 2155
De Marchi, G., Paresce, F., & Pulone, L. 2007, ApJ, 656, L65
Dokuchaev, V. I. & Ozernoi, L. M. 1985, Soviet Astronomy Letters, 11, 139
Duquennoy, A. & Mayor, M. 1991, A&A, 248, 485
Dull, J. D., Cohn, H. N., Lugger, P. M., Murphy, B. W., Seitzer, P. O., Callanan, P. J., Rutten, R. G. M. & Charles, P. A. 1997, ApJ, 481, 267
Eichler, D. et al. 1989, Nature, 340, 126
Fabian, A. C., Pringle, J. E. & Rees, M. J. 1975, MNRAS, 172, 15
Faber, J.A., Grandclément, P., Rasio, F.A. 2002, Phys. Rev. Letters, 89, 231102
Faber, S. M. et al. 2007, ApJ, 665, 265
Fox, D. B. et al. 2005, Nature, 437, 845
Frank, J. 1978, MNRAS, 184, 87
Fregeau, J. M. 2008, ApJ, 673, L25
Freiburgaus, C., Rosswog, S., Thielemann, F.-K. 1999, ApJ, 525, L121
Fryer, C. L., Woosley, S. E., & Hartmann, D. H. 1999, ApJ, 526, 152
Gal-Yam, A. et al., 2008, ApJ, 686, 408
Gehrels, N. et al. 2005, Nature, 437, 851
Gehrels, N., Ramirez-Ruiz, E., Fox, D.B. 2009, ARA&A, 47, 567
Graham, J. F., et al. 2009, ApJ, 698, 1620
Gnedin, O. Y., Lee, H. M., & Ostriker, J. P. 1999, ApJ, 522, 935
Georgiev, I. Y., Hilker, M., Puzia, T. H., Goudfrooij, P., & Baumgardt, H. 2009, MNRAS, 647
Giersz, M. & Heggie, D. C. 2009, MNRAS, 395, 1173
Goodman, J. 1987, ApJ, 313, 576
Grindlay, J., Portegies Zwart, S. & McMillan, S. 2006, Nature Physics, 2, 116
Guetta, D., Piran, T. 2005, A&A, 435, 421
Guetta, D. & Piran, T. 2006, A&A, 453, 823
Hansen, B.M.S., Murali, C. 1998, ApJ, 505, L15
Heggie, D. C. 1975, MNRAS, 173, 72
Heggie, D. C. 1985, in IAU Symposium, Vol. 113, Dynamics of Star Clusters, ed. J. Goodman & P. Hut, 139–157
Heggie, D. C. & Giersz, M. 2008, MNRAS, 389, 1858
—. 2009, MNRAS, 397, L46
Heggie, D. C. & Ramamani, N. 1989, MNRAS, 237, 757
Heggie, D. C., Trenti, M., & Hut, P. 2006, MNRAS, 368, 677
Heinke, C., et al., 2006, ApJ, 651, 1098
Hénon, M. 1965, Annales d'Astrophysique, 28, 62
Hessels, J. W. T., Ransom, S. M., Stairs, I. H., Freire, P. C. C.,Kaspi, V.M., Camilo, F. 2006, Science, 311, 1901
Hills, J. G. 1975, AJ, 80, 809
Hjorth, J. et al. 2005, Nature, 437, 859
Hopkins, A. M. & Beacom, J. F. 2006, ApJ, 651, 142
Hopman, C., Guetta, D., Waxman, E., & Portegies Zwart, S. 2006, ApJ, 643, L91
Hurley, J. R., Aarseth, S. J., & Shara, M. M. 2007, ApJ, 665, 707
Hut, P., & Verbunt, F. 1983, Nature, 301, 587
Hut, P., McMillan, S., Goodman, J., Mateo, M., Phinney, E. S., Pryor, C., Richer, H. B., Verbunt, F., & Weinberg, M. 1992, PASP, 104, 981
Inagaki, S. & Lynden-Bell, D. 1983, MNRAS, 205, 913

Ivanova, N., Heinke, C. O., Rasio, F. A., Belczynski, K., & Fregeau, J. M. 2008, MNRAS, 386, 553
Janka, T. & Ruffert, M. 1996, A&A, 307, L33
Jordán, A. et al. 2005, ApJ, 634, 1002
Jordán, A. et al. 2006, ApJ, 651, L25
Kalogera, V., Kim, C., Lorimer, D. R., Burgay, M., D'Amico, N., Possenti, A., Manchester, R. N., Lyne, A. G., Joshi, B. C., McLaughlin, M. A., Kramer, M., Sarkissian, J. M., & Camilo, F. 2004, ApJ, 601, L179
Kandrup, H. E. 1990, ApJ, 364, 100
Katz, J. I. 1975, Nature, 253, 698
Kim, S. S. & Lee, H. M. 1999, A&A, 347, 123
Kochanek, C. S. 1992, ApJ, 385, 604
Kluźniak, W. Ruderman, M. 1998, ApJ,
Lacy, J.H., Townes, C.H., Hollenbach, D.K. 1982, ApJ, 262, 120
Lai, D., Rasio, F.A., Shapiro S.L. 1993a, ApJ, 406 L63
Lai, D., Rasio, F.A., Shapiro S.L. 1993b, ApJS, 88, 205
Lattimer, J.M., Schramm, D.N. 1974, ApJ, 192, L145
Lattimer, J.M., Schramm, D.N. 1976, ApJ, 210, 549
Lee, H. M., & Ostriker, J. P. 1986, ApJ, 310, 176
Lee, W.H., Kluzniak, W. 1999, ApJ, 526, 178
Lee, W.H., Ramirez-Ruiz, E., Granot, J. 2005, ApJ, 630, L165
Lee, W.H. Ramirez-Ruiz, E. 2007, New. J. Phys. 9. 17
Lee, W. H., Ramirez-Ruiz, E. & Lopez-Camara, D. 2009, ApJ, 699, L93
Lee, W.H. 2000, MNRAS, 318, 606
Lee, W.H. 2001, MNRAS, 328, 583
Lynden-Bell, D. & Eggleton, P. P. 1980, MNRAS, 191, 483
McLaughlin, D. E. 1999, AJ, 117, 2389
McLaughlin, D. E. 2000, ApJ, 539, 618
McLaughlin, D. E. & Fall, S. M. 2008, ApJ, 679, 1272
McMillan, S. L. W., McDermott, P. N., & Taam, R. E. 1987, ApJ, 318, 261
Mcnamara, B.J.., Harrison, T. E., Baumgardt, H. 2004, ApJ, 602, 264
Merritt, D. 2009, ApJ, 694, 959
Metzger, B. D., Arcones, A., Quataert, E., Martinez-Pinedo, G. 2010, MNRAS, 402, 2771
Monaghan, J.J. 1992, ARA&A, 30, 543
Moore, B., Diemand, J., Madau, P., Zemp, M., & Stadel, J. 2006, MNRAS, 368, 563
Nakar, E. et al 2006, ApJ, 650, 281
Nakar, E. 2007, Physics Reports, 442, 166
Narayan, R., Piran, T., & Shemi, A. 1991, ApJ, 379, L17
Noyola, E. & Gebhardt, K. 2006, AJ, 132, 447
O'Shaughnessy, R., Kim, C., Fragos, T., Kalogera, V., Belczynski, K., 2005, ApJ, 633, 1076
O'Shaughnessy, R., Belczynski, K., Kalogera, V., 2008, ApJ, 675, 566
O'Shaughnessy, R., Kalogera, V., Belczynski, K., 2010, ApJ, 716, 615
Paczyński, B. 1971, ARA&A, 9, 183
Paczyński, B. 1986, ApJ, 308, L43
Paczyński, B., Wiita, P.J. 1980, A&A, 88, 23
Parsons, R.K., Ramirez-Ruiz, E., Lee, W.H. 2009, ApJ submitted, arXiv:0904.1768
Pedersen, K., et al. 2005, ApJ, 634, L17
Phinney, E. S. 1991, ApJ, 380, L17
Pooley, D, et al., 2003, ApJ, 591, L131
Press, W. H. & Teukolsky, S. A. 1977, ApJ, 213, 183
Price, D. Rosswog, S. 2006, Science, 312, 719
Prochaska, J. X. et al. 2006, ApJ, 642, 989
Quinlan, G. D. 1996, New Astronomy, 1, 255
Rasio, F.A., Shapiro S.L. 1991, ApJ, 377, 559
Rasio, F.A., Shapiro S.L. 1992, ApJ, 401, 226
Rasio, F.A., Shapiro S.L. 1994, ApJ, 432, 242
Raskin, C., Timmes, F.X., Scannapieco, E., Diehl, S., Fryer, C. 2009, MNRAS, 399, L159
Rauch, K. P. & Tremaine, S. 1996, New Astronomy, 1, 149
Rees, M.J. 1988, Nature, 333, 523
Rosswog, S., Ramirez-Ruiz, E., Davis, M.B. 2003, MNRAS, 345, 1077
Rosswog, S. 2005, ApJ, 634, 1202
Rosswog, S. 2007, MNRAS, 376, L48
Rosswog, S., Kasen, D., Guillochon, J., Ramirez-Ruiz, E. 2009, ApJ, 705, L128
Salvaterra, R., Cerutti, A., Chincarini, G., Colpi, M., Guidorzi, C., & Romano, P. 2008, MNRAS, 388, L6
Seth, A., Agüeros, M., Lee, D., & Basu-Zych, A. 2008, ApJ, 678, 116
Shapiro, S. L. 1977, ApJ, 217, 281
Shibata, M., Taniguchi. K. 2006, Phys. Rev. D, 73, 064027
Sigurdsson, S. & Phinney, E. S. 1993, ApJ, 415, 631
Soderberg, A. M., Berger, E., Kasliwal, M., Frail, D. A., Price, P. A., Schmidt, B. P., Kulkarni, S. R., Fox, D. B., Cenko, S. B., Gal-Yam, A., Nakar, E., & Roth, K. C. 2006, ApJ, 650, 261
Symbalisty, E.M.D., Schramm, D.N., 1982, ApJ, 1982, 22, L143
Usov, V.V. 1992, Nature, 357, 472
van den Bosch, R., de Zeeuw, T., Gebhardt, K., Noyola, E., & van de Ven, G. 2006, ApJ, 641, 852
Vesperini, E. & Heggie, D. C. 1997, MNRAS, 289, 898
Walcher, C. J., Böker, T., Charlot, S., Ho, L. C., Rix, H.-W., Rossa, J., Shields, J. C., & van der Marel, R. P. 2006, ApJ, 649, 692
Walcher, C. J., van der Marel, R. P., McLaughlin, D., Rix, H.-W., Böker, T., Häring, N., Ho, L. C., Sarzi, M., & Shields, J. C. 2005, ApJ, 618, 237
Zemp, M., Ramirez-Ruiz, E., Diemand, J. 2009, ApJ, 705, L186
Zheng, Z., Ramirez-Ruiz, E. 2007, ApJ, 665, 1220